Distinct functions of macrophage-derived and cancer cell-derived cathepsin Z combine to promote tumor malignancy via interactions with the extracellular matrix

Leila Akkari,[1] Vasilena Gocheva,[1] Jemila C. Kester,[1] Karen E. Hunter,[1] Marsha L. Quick,[1] Lisa Sevenich,[1] Hao-Wei Wang,[1] Christoph Peters,[2,3,4] Laura H. Tang,[5] David S. Klimstra,[5] Thomas Reinheckel,[2,3,4] and Johanna A. Joyce[1]

[1]Cancer Biology and Genetics Program, Memorial Sloan-Kettering Cancer Center, New York, New York,10065, USA; [2]Institute of Molecular Medicine and Cell Research, Albert-Ludwigs University, D-79104 Freiburg, Germany; [3]BIOSS Centre for Biological Signalling Studies, D-79104 Freiburg, Germany; [4]German Cancer Consortium (DKTK), D-79104 Freiburg, Germany; [5]Pathology Department, Memorial Sloan-Kettering Cancer Center, New York, New York 10065, USA

During the process of tumor progression, cancer cells can produce the requisite growth- and invasion-promoting factors and can also rely on noncancerous cells in the tumor microenvironment as an alternative, cell-extrinsic source. However, whether the cellular source influences the function of such tumor-promoting factors remains an open question. Here, we examined the roles of the cathepsin Z (CtsZ) protease, which is provided by both cancer cells and macrophages in pancreatic neuroendocrine tumors in humans and mice. We found that tumor proliferation was exclusively regulated by cancer cell-intrinsic functions of CtsZ, whereas tumor invasion required contributions from both macrophages and cancer cells. Interestingly, several of the tumor-promoting functions of CtsZ were not dependent on its described catalytic activity but instead were mediated via the Arg–Gly–Asp (RGD) motif in the enzyme prodomain, which regulated interactions with integrins and the extracellular matrix. Together, these results underscore the complexity of interactions within the tumor microenvironment and indicate that cellular source can indeed impact molecular function.

[*Keywords*: cell invasion; cell migration; tumor microenvironment; protease]

Supplemental material is available for this article.

Received July 26, 2014; revised version accepted August 29, 2014.

Tumors arise in complex tissue microenvironments in which a multitude of different noncancerous cell types can potently regulate disease initiation and progression (Hanahan and Coussens 2012; Quail and Joyce 2013). In addition, interactions with the extracellular matrix (ECM) are critical for modulating cell behavior, including enhancing cell survival and promoting invasion via ECM turnover and proteolysis (Lu et al. 2012; Sevenich and Joyce 2014). The ECM is a heterogeneous mix of proteins and polysaccharides, including different collagens, laminins, fibronectin, and heparan sulfate proteoglycans, which form an intricate network that confers tissue structure and regulates growth factor availability (Hynes and Naba 2012; Lu et al. 2012). Integrins are central in mediating interactions between cells and the surrounding ECM, and integrin engagement at the cell surface results in activation of downstream signaling nodes, including focal adhesion kinase (FAK) and Src kinase, to promote cancer cell proliferation, survival, migration, and invasion (Desgrosellier and Cheresh 2010; Huttenlocher and Horwitz 2011; Moreno-Layseca and Streuli 2014).

Among the noncancerous cell types that modulate tumorigenesis, tumor-associated macrophages (TAMs) have emerged as critical regulators of tumor progression

Corresponding author: joycej@mskcc.org
Article is online at http://www.genesdev.org/cgi/doi/10.1101/gad.249599.114.

and metastasis (Biswas et al. 2013; Noy and Pollard 2014). This is particularly evident in tumor invasion, as TAMs provide a major source of proteases that modulate the ECM (Joyce and Pollard 2009). In determining the mechanisms by which TAMs promote different tumorigenic processes, the focus to date has been predominantly centered on identifying factors that are TAM-specific or TAM-enriched, which are not necessarily provided by the cancer cells. TAMs may thus represent an alternative cellular source for the tumor to have access to such growth- and invasion-promoting factors. However, the possibility that tumorigenic factors are supplied by both cancer cells and TAMs to confer distinct functions or activate different signaling pathways depending on the specific cellular source merits further investigation.

To explore this hypothesis, we examined the functions of cathepsin X/Z, a cysteine cathepsin protease, which is produced by both cancer cells and TAMs in the microenvironment of pancreatic neuroendocrine tumors (PanNETs) in patients and mice, as we show here. Cathepsin X/Z has been referred to by both names following its initial discovery and characterization (Nagler and Menard 1998; Santamaria et al. 1998; Nagler et al. 1999; Deussing et al. 2000); however as the official gene name is *cathepsin Z*, we use this nomenclature throughout. Cathepsin Z (CtsZ) is a member of the cysteine cathepsin protease family, which is comprised of 11 members in humans: cathepsins B, C, H, F, K, L, O, S, L2/V, W, and Z (Turk et al. 2012). While most cathepsins are predominantly endopeptidases, CtsZ is an exopeptidase, with strict carboxypeptidase activity (Nagler et al. 1999; Turk et al. 2012). CtsZ additionally has the unique feature of an exposed integrin-binding Arg–Gly–Asp (RGD) motif within the propeptide of the enzyme (Nagler and Menard 1998; Sivaraman et al. 2000; Lechner et al. 2006), which is cleaved and removed following its activation. Through the RGD motif, CtsZ has been shown to interact with several integrins during normal homeostasis, including αvβ3 (Kos et al. 2009). CtsZ–integrin interactions have been reported in different immune processes, including dendritic cell maturation (Obermajer et al. 2008b) and lymphocyte invasion and proliferation (Jevnikar et al. 2008; Obermajer et al. 2008a). However, whether engagement with integrins is important for any role of CtsZ in cancer and the relative importance of its proteolytic versus nonproteolytic functions have not been investigated to date. Moreover, compared with other cathepsins, relatively little is known about the roles of CtsZ in cancer. Analysis of patient samples has revealed a correlation between high CtsZ expression levels and advanced malignancy in hepatocellular carcinomas and colorectal, gastric, and prostate cancer (Hidaka et al. 2000; Nagler et al. 2004; Krueger et al. 2005; Wang et al. 2011; Vizin et al. 2012), suggesting potential cancer-promoting functions in different tumor microenvironments.

To investigate the relative roles of CtsZ in TAMs and cancer cells in vivo, we used the RIP1-Tag2 (RT2) PanNET model, in which the SV40 T antigen (Tag) viral oncogene is specifically expressed in β cells of the pancreatic islets under the control of the rat insulin promoter (RIP) (Hanahan 1985). SV40 Tag expression inactivates p53 and pRb, resulting in the development of PanNETs through a stereotypical progression from hyperplastic islets to angiogenic islets and finally multiple end-stage tumors. While human PanNETs are not driven by viral oncogenes, negative regulators of both the p53 and pRb pathways are altered in PanNET patients, resulting in attenuated tumor suppressor function (Hu et al. 2010; Tang et al. 2012). Moreover, in preclinical studies, the RT2 model has been shown to have a predictive value for clinical outcome (Tuveson and Hanahan 2011), indicating that at least some important characteristics are shared between RT2 mice and PanNET patients.

The RT2 model has also proven invaluable for investigating multistep tumor progression and exploring interactions between cancer cells and their microenvironment. For example, we used this model to identify novel roles for individual cysteine cathepsin family members in different stages of tumor development. Specifically, we found that six cathepsins (B, C, H, L, S, and Z) were up-regulated during RT2 tumorigenesis (Joyce et al. 2004). We individually deleted each of these cathepsins in the RT2 model and identified different roles for CtsB, CtsH, CtsL, and CtsS in angiogenesis, tumor growth, and/or invasion (Gocheva et al. 2006, 2010a; Gocheva and Joyce 2007). CtsC, which was similarly up-regulated during RT2 tumorigenesis, had no impact on any aspect of cancer progression when deleted (Gocheva et al. 2006).

Here, we report the analysis and identification of novel functions for the remaining up-regulated family member, CtsZ, in PanNET tumorigenesis. Given the unique characteristics of CtsZ relative to other cathepsin family members, including the presence of a RGD motif in the prodomain and its enzymatic function being exclusively as a carboxypeptidase, we sought to determine whether it has distinctive tumorigenic functions in the RT2 model. We used the complementary genetic approaches of gene deletion, bone marrow (BM) transplantation (BMT), and somatic gene transfer in RT2 mice to show that cancer cell-supplied CtsZ promotes cancer cell invasion and growth, while TAM-produced CtsZ is critical for enhancing tumor invasion. Importantly, we show that several of the tumor-promoting functions of CtsZ are independent of its catalytic activity and are instead mediated via the RGD motif, engagement of integrins, and subsequent activation of FAK–Src signaling in cancer cells—a function that has not been previously described for this protease in the context of cancer.

Results

CtsZ is supplied by both macrophages and cancer cells and correlates with human PanNET malignancy

We first characterized the expression pattern of CtsZ in wild-type RT2 tumors by coimmunostaining with antibodies recognizing epitopes on cancer cells (synaptophysin [SYP]), TAMs (CD68), endothelial cells (CD31), or pericytes (NG2). We found that CtsZ expression was highly

enriched in TAMs and also expressed in cancer cells (Fig. 1A; Supplemental Fig. S1A). In contrast, there was no evident colocalization with the other cell types present in RT2 tumors. These results were confirmed by quantitative PCR (qPCR) analysis of *CtsZ* expression in sorted cancer cells and TAMs from wild-type RT2 tumors (Supplemental Fig. S1B).

To address the broader relevance of CtsZ in PanNET development, we examined its expression in human PanNETs as they progress to advanced malignancy. A

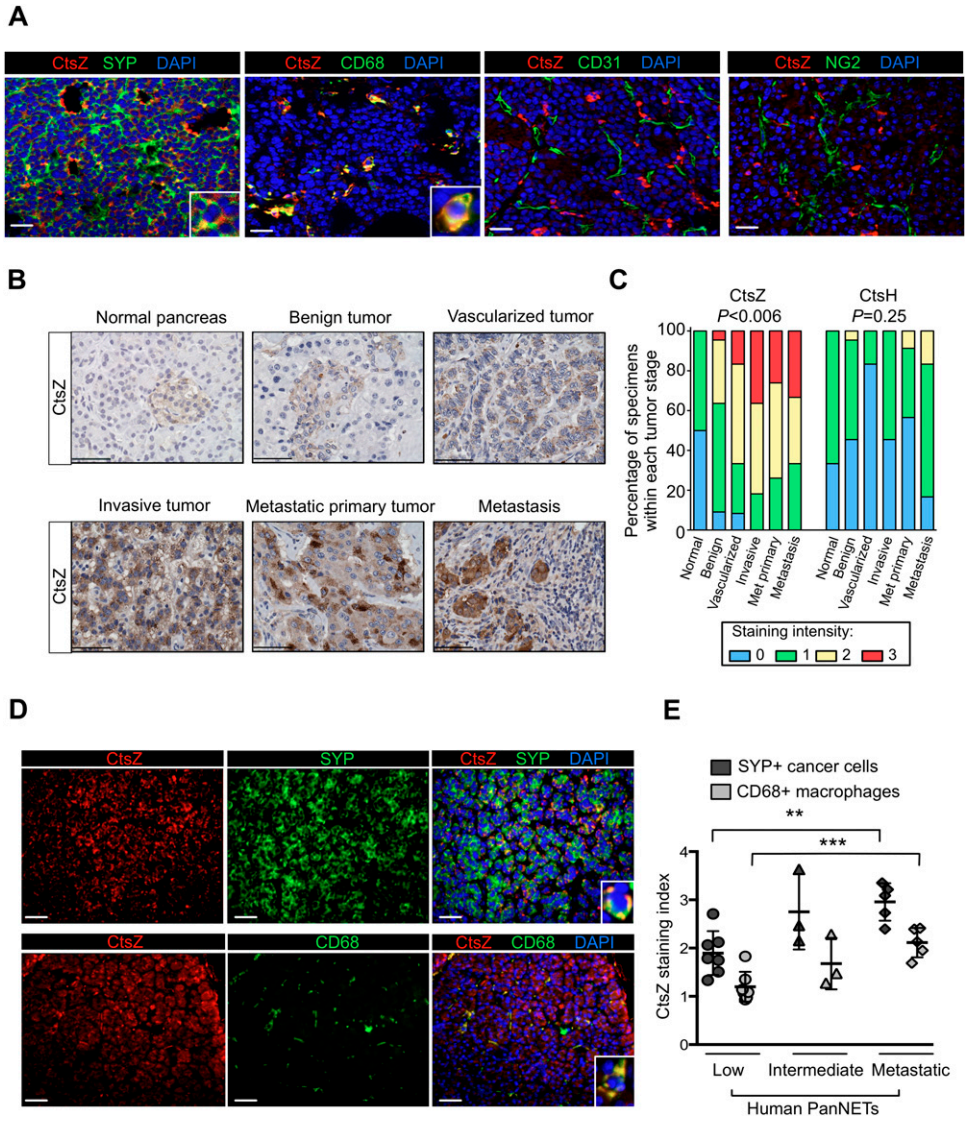

Figure 1. CtsZ is produced by both macrophages and cancer cells in mouse and human PanNETs, and high levels positively correlate with tumor malignancy. (*A*) CtsZ is expressed by macrophages and cancer cells in the RT2 mouse model of PanNET. Antibodies against CtsZ and cell type-specific markers for cancer cells (SYP), macrophages (CD68), endothelial cells (CD31), and pericytes (NG2) were used to identify cells expressing CtsZ within wild-type (WT) RT2 tumors. (*B*) Tissue microarrays (TMAs) constructed from a panel of ~80 human PanNETs and normal pancreatic tissues were stained with antibodies against CtsZ (brown). Hematoxylin (blue) was used as a counterstain. Representative images of CtsZ staining are shown from the different stages of tumor progression included on the TMA. (*C*) Staining intensity of CtsZ or CtsH (negative control) for each specimen on the TMA was scored as negative (0) or positive (three levels: weak [1], moderate [2], and strong [3]). Staining intensities were graphed as the percentage of the total numbers of samples on the TMA within each tumor stage. For each cathepsin, an overall statistical test of differences among any of the groups (normal and tumor) was performed. An exact version of Mantel Haenszel's test for trend was performed to analyze differences in staining in each tumor group compared with the normal controls and calculate *P*-values, which are shown *above* each data set. (*D*) Representative images from a panel of whole-tissue samples from 15 PanNET patients costained with CtsZ (red) and CD68 (green) or SYP (green). These samples represent a different series than the TMA samples in *B*, and patient information can be found in Supplemental Table 1. (*E*) Quantification of the CtsZ staining index was determined as a measure of relative CtsZ levels in cancer cells and macrophages in low-grade, intermediate-grade, and metastatic PanNETs. Statistical significance was calculated by an unpaired two-tailed Student's *t*-test; (**) $P < 0.01$; (***) $P < 0.001$. Graphs show mean ± SEM. Bars in all panels, 50 μm.

tissue microarray (TMA) composed of normal pancreas tissue controls and 80 PanNET lesions, the majority of which were insulinomas and associated metastatic lesions (Gocheva et al. 2006), was used to perform immunostaining for CtsZ (Fig. 1B), followed by blinded scoring of each lesion based on staining intensity (Fig. 1C). We found that CtsZ was progressively up-regulated as PanNETs advance to higher grades, when compared with normal islets and the normal exocrine pancreas. We included CtsH staining here as a negative control, as its deletion in the RT2 model did not affect tumor invasion (Gocheva et al. 2010a). CtsH immunostaining was only weakly positive in human PanNET lesions and did not show any significant association with tumor malignancy. CtsZ expression and localization in human PanNETs was consistent with immunostaining of RT2 tumors, with both SYP$^+$ cancer cells and CD68$^+$ TAMs expressing the protease (Fig. 1D). These results also revealed a gradual increase in CtsZ expression in both cancer cells and TAMs in the progression from low-grade to metastatic PanNETs in patients (Fig. 1E).

We next sought to determine the functional contribution of CtsZ to tumor formation and progression by crossing *CtsZ*$^{-/-}$ mice (Sevenich et al. 2010) into the RT2 background. We first confirmed that *CtsZ* mRNA expression was indeed absent in the *CtsZ*$^{-/-}$ RT2 tumors and that expression of other cathepsin family members (*CtsB*, *CtsH*, *CtsL*, and *CtsS*) did not change between *CtsZ*$^{-/-}$ and wild-type RT2 tumors (Supplemental Fig. S2A). We then analyzed the frequency of angiogenic islets. These premalignant lesions undergo extensive vascularization, which is required for subsequent expansive tumor growth. The average number of angiogenic islets in *CtsZ*$^{-/-}$ RT2 mice decreased by 53% compared with wild-type RT2 controls (Fig. 2A, assessed at 10.5 wk of age), indicating a critical role for CtsZ in tumor

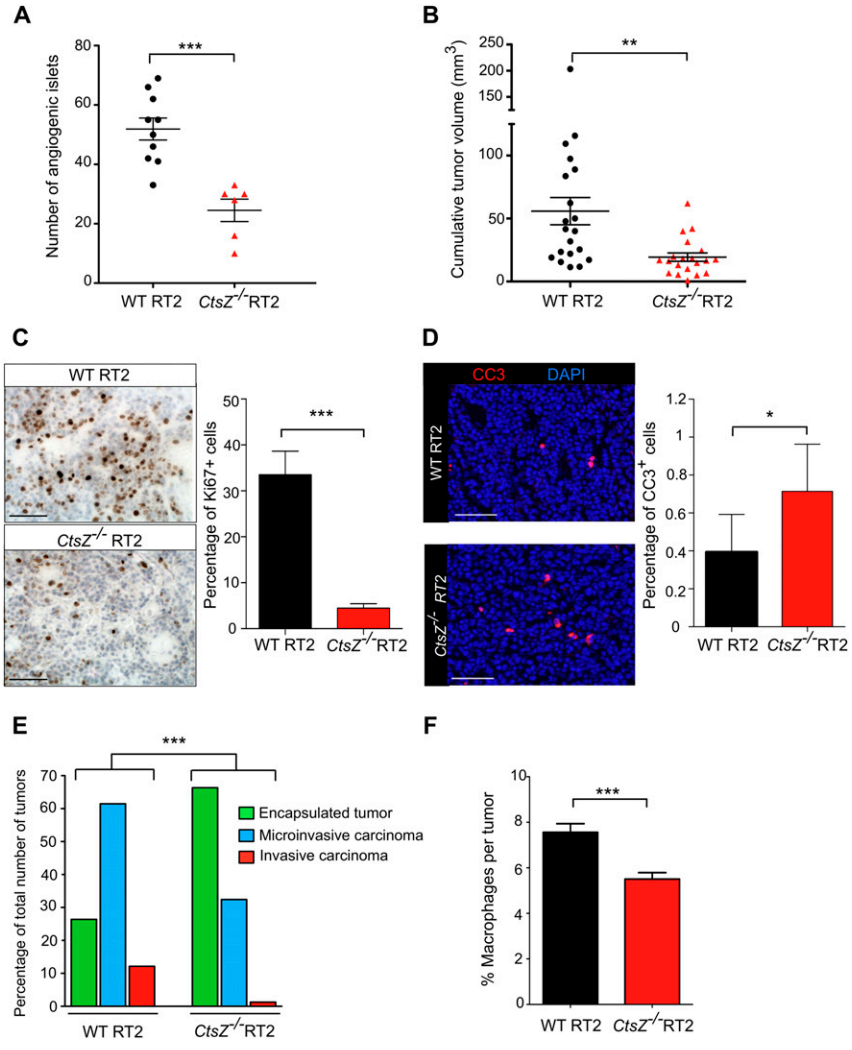

Figure 2. *CtsZ* deficiency impairs multiple tumorigenic processes in the RT2 PanNET model. (*A*) Angiogenic switching was assessed in 10.5-wk-old wild-type (WT) RT2 or *CtsZ*$^{-/-}$ RT2 mice (n = 10 and n = 6 mice, respectively) by manually counting the number of angiogenic islets in the pancreas. The graph shows the average number of angiogenic islets per mouse. (*B*) Cumulative tumor volume, represented as the sum of the volumes of all tumors per mouse, was calculated for 13.5-wk-old wild-type RT2 or *CtsZ*$^{-/-}$ RT2 mice (n = 20 per group). (*C*) Representative images and quantitation of Ki67 staining (brown) in wild-type and *CtsZ*$^{-/-}$ RT2 tumors showing an 86% decrease in cell proliferation in tumors deficient for *CtsZ*. Tumors from five wild-type RT2 and six *CtsZ*$^{-/-}$ RT2 mice were analyzed. (*D*) Representative images and quantitation of cleaved caspase 3 (CC3) staining (red) in wild-type and *CtsZ*$^{-/-}$ RT2 tumors revealed a 1.8-fold increase in apoptosis in tumors deficient for *CtsZ*. Tumors from 11 wild-type RT2 and six *CtsZ*$^{-/-}$ RT2 mice were analyzed. (*E*) Graph showing the relative proportions of encapsulated, microinvasive, and invasive carcinomas in wild-type RT2 versus *CtsZ*$^{-/-}$ RT2 mice at 13.5 wk of age. In total, 112 tumors from 15 wild-type RT2 mice and 103 tumors from 16 *CtsZ*$^{-/-}$ RT2 mice were analyzed. (*F*) Quantification of CD68$^+$ macrophages in wild-type RT2 or *CtsZ*$^{-/-}$ RT2 tumors relative to the total number of DAPI$^+$ cells showed a significant decrease in macrophages in *CtsZ*$^{-/-}$ tumors. n = 41 tumors analyzed per genotype. Graphs show mean ± SEM. Statistical significance was calculated by unpaired two-tailed Student's t-test (*A–D,F*) or using a cumulative logit model with generalized estimating equations to correct for correlations within individual mice (*E*). (*) $P < 0.05$; (**) $P < 0.01$; (***) $P < 0.001$. Bars: *C,D*: 50 μm.

initiation. We analyzed a separate cohort of animals at end stage (13.5 wk of age) and found that cumulative tumor volume was reduced by 63% in $CtsZ^{-/-}$ RT2 mice (Fig. 2B), although the number of tumors per animal at this time point was not altered (Supplemental Fig. S2B). The reduction in tumor burden was associated with an increase in overall survival of $CtsZ^{-/-}$ RT2 mice (Supplemental Fig. S2C).

Phenotypic analysis of several key tumorigenic properties, including proliferation, vascular density, invasion, and evasion of apoptosis, revealed that $CtsZ^{-/-}$ RT2 tumors displayed significant defects in multiple processes. The proliferation index of wild-type and $CtsZ^{-/-}$ RT2 tumors was assessed by Ki67 staining and was reduced by 86% in $CtsZ^{-/-}$ lesions (Fig. 2C). The apoptotic index was determined by cleaved caspase 3 (CC3) staining and increased by 1.8-fold in $CtsZ^{-/-}$ RT2 tumors (Fig. 2D). Furthermore, deletion of *CtsZ* significantly reduced the incidence of both microinvasive and frankly invasive carcinomas using a well-established grading scheme (Lopez and Hanahan 2002). The lesions that did form in $CtsZ^{-/-}$ animals were predominantly low-grade encapsulated tumors (Fig. 2E). Interestingly, although vessel density was equivalent between $CtsZ^{-/-}$ and wild-type tumors (Supplemental Fig. S2D), TAM numbers were decreased by 23% (Fig. 2F), suggesting a defect in the capacity of $CtsZ^{-/-}$ macrophages to infiltrate the tumor. Collectively, these results show that deletion of *CtsZ* resulted in substantially reduced initiation, growth, and malignancy of PanNETs through a combined effect of blocking proliferation and invasion and increasing apoptosis.

Complementary roles of cancer cell-derived and TAM-derived CtsZ

We performed BMT experiments to explore the relative contribution of TAM-derived and cancer cell-derived CtsZ in tumor progression, given its expression in both cell compartments. We showed previously that the vast majority (88%) of BM-derived cells in RT2 tumors differentiate into macrophages (Gocheva et al. 2010b), and thus BMT provides a strategy to experimentally manipulate the expression of TAM-supplied CtsZ in vivo. We transplanted β-actin-GFP$^+$ wild-type or $CtsZ^{-/-}$ donor BM into otherwise $CtsZ^{-/-}$ RT2 or wild-type RT2 recipients, respectively (Fig. 3A), as previously described for other cathepsin family members (Gocheva et al. 2010b). Analysis of end-stage cumulative tumor volume in wild-type RT2 mice that underwent transplantation with wild-type or $CtsZ^{-/-}$ BM revealed no significant differences (Fig. 3B). In accordance with these results, transplantation of wild-type BM into $CtsZ^{-/-}$ RT2 mice did not rescue their diminished tumor burden, suggesting that the growth-promoting functions of this protease are likely cancer cell-intrinsic.

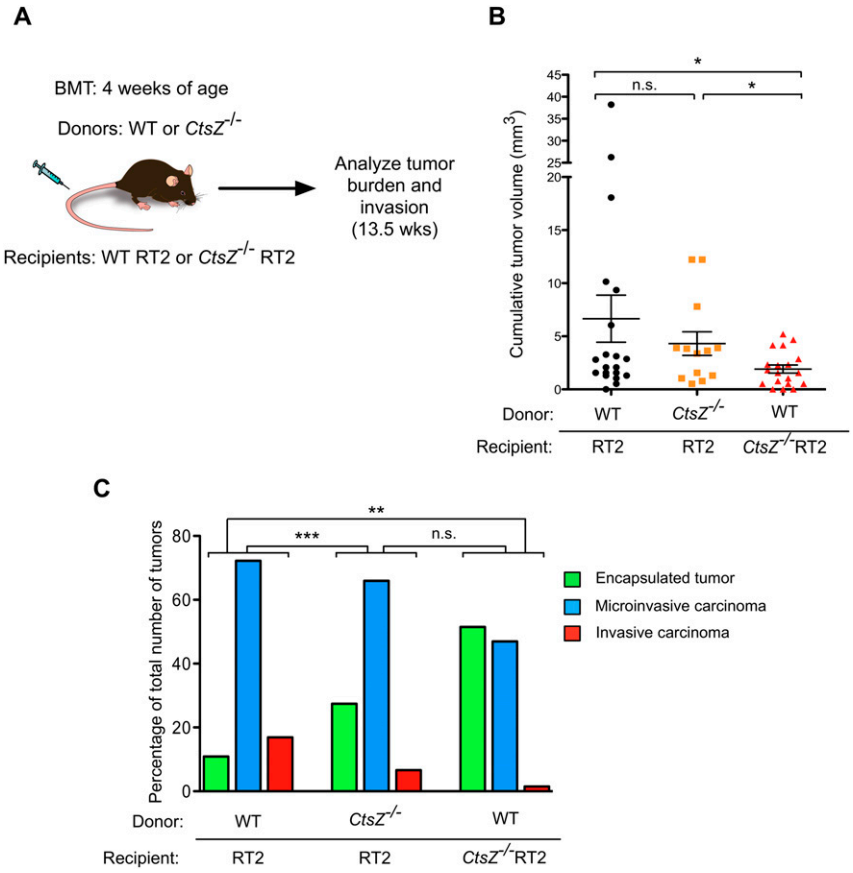

Figure 3. Macrophage-derived CtsZ promotes tumor invasion but does not alter tumor growth. (*A*) Schematic of the BMT experimental design. (*B*) Cumulative tumor volume, represented as the sum of the individual tumor volumes per mouse, was calculated in 13.5-wk-old $CtsZ^{-/-}$ RT2 and wild-type (WT) RT2 recipient mice transplanted with wild-type or $CtsZ^{-/-}$ donor BM (β-actin-GFP$^+$), respectively. The total number of BMT recipient mice analyzed were as follows: n = 17 wild-type BM → wild-type RT2, n = 13 $CtsZ^{-/-}$ BM → wild-type RT2, and n = 14 wild-type BM → $CtsZ^{-/-}$ RT2. (*C*) Hematoxylin and eosin (H&E) staining was used to grade tumors from BM-transplanted wild-type RT2 or $CtsZ^{-/-}$ RT2 mice. Graph showing the relative proportions of encapsulated, microinvasive, and invasive carcinomas in transplanted mice from both genotypes. Deletion of *CtsZ* in the BM resulted in a substantial decrease in tumor invasion compared with the wild-type BM into wild-type RT2 recipient group. The total number of BMT recipient mice analyzed were as follows: 11 wild-type BM → wild type (88 tumors), 13 $CtsZ^{-/-}$ BM → wild type (70 tumors) and seven wild-type BM → $CtsZ^{/-}$ (21 tumors). Graphs show mean ± SEM in *B*. Statistical significance was calculated by unpaired two-tailed Student's *t*-test in *B* or using the cumulative logit model in *C*; (n.s.) nonsignificant; (*) $P < 0.05$; (**) $P < 0.01$; (***) $P < 0.001$.

In contrast, depletion of TAM-derived CtsZ significantly reduced the proportion of invasive lesions in wild-type RT2 recipients, indicating that the invasion-promoting functions of CtsZ are at least in part TAM-derived (Fig. 3C). Accordingly, transfer of wild-type BM into *CtsZ*$^{-/-}$ RT2 mice partially restored tumor invasion to the wild-type RT2 spectrum of grades (Fig. 3C). Together, these results indicate that TAM-derived CtsZ supports increased tumor invasiveness, whereas cancer cell CtsZ is critical for regulating both tumor growth and invasion.

While the BMT experiments allowed us to specifically manipulate TAM-supplied CtsZ and evaluate its impact on regulating invasion, we devised a complementary in vivo approach to investigate how CtsZ expression in cancer cells favors tumor growth and progression to malignancy by reintroducing its expression specifically in cancer cells in an otherwise *CtsZ*$^{-/-}$ host. This strategy employed the RCAS-Tva system of somatic gene transfer that enables delivery of genes in a cell type-specific and temporally regulated manner (Fisher et al. 1999). We crossed RT2 animals with RIP-*Tva* transgenic mice, which allowed for retroviral-based gene delivery specifically to Tva^{+} tumor-initiating β cells of the pancreas (Du et al. 2007). Intracardiac injection of RIP-*Tva*; RT2 mice with RCAS viruses prior to tumor development, at 7 wk of age, has been shown to result in successful infection of hyperplastic cells (Du et al. 2007).

We delivered either RCAS-*CtsZ* or the control RCAS-*GFP* virus into recipient RIP-*Tva*; *CtsZ*$^{-/-}$ RT2 animals as schematized in Figure 4A. We first confirmed

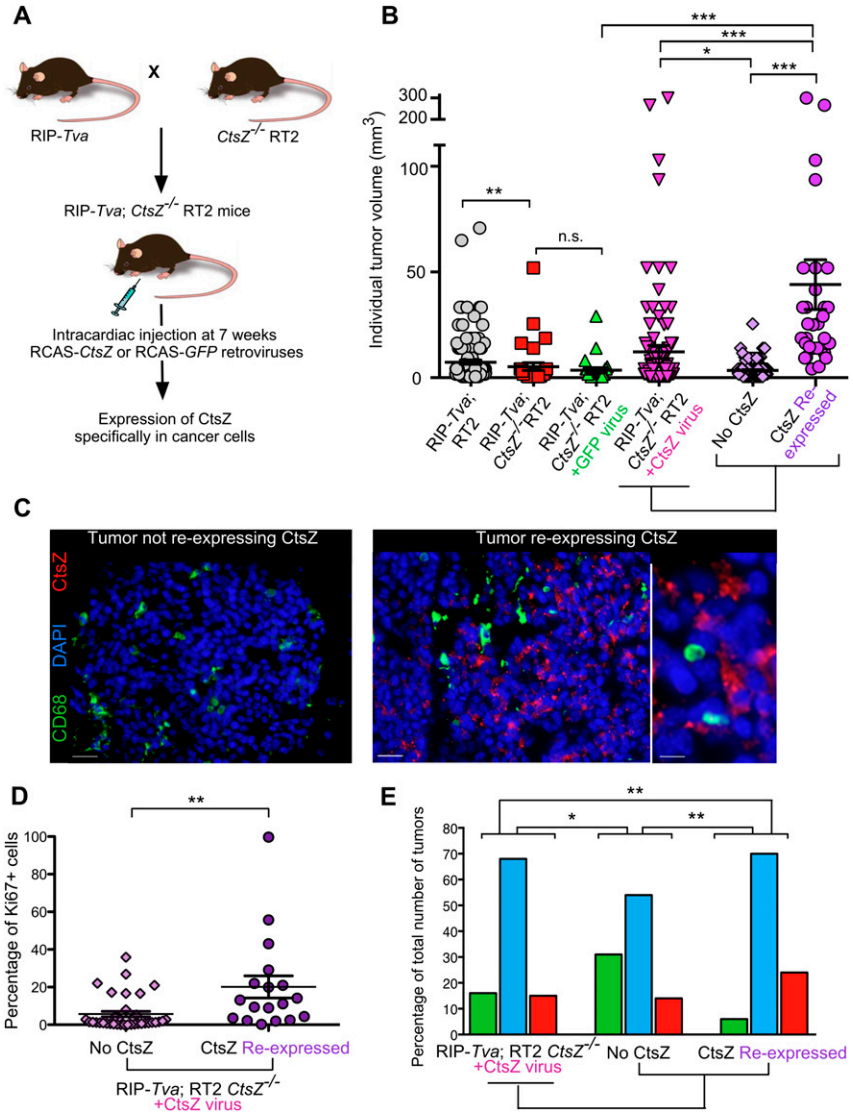

Figure 4. Cancer cell-derived CtsZ regulates tumor growth and invasion. (*A*) Schematic of the experimental design to specifically express CtsZ in cancer cells in vivo. RIP-*Tva* and *CtsZ*$^{-/-}$ RT2 mice were crossed to generate RIP-*Tva*; *CtsZ*$^{-/-}$ RT2 mice. These mice express the Tva receptor for the RCAS avian retrovirus specifically in β cells of the pancreas, which give rise to PanNETs. RCAS-*CtsZ* or RCAS-*GFP* viruses were produced and concentrated in vitro, followed by intracardiac injection into RIP-*Tva*; *CtsZ*$^{-/-}$ RT2 mice at 7 wk of age. Mice were aged and sacrificed at 13.5 wk for further characterization. (*B*) Graph showing the volumes of individual tumors from RIP-*Tva*; RT2 and RIP-*Tva*; *CtsZ*$^{-/-}$ RT2 mice or RIP-*Tva*; *CtsZ*$^{-/-}$ RT2 animals injected with the RCAS-*GFP* or RCAS-*CtsZ* virus (13.5 wk of age). Individual tumors from RIP-*Tva*; *CtsZ*$^{-/-}$ RT2 mice (n = 141) injected with the RCAS-*CtsZ* virus were categorized according to whether they re-expressed CtsZ (n = 32) or not (n = 109), and tumors re-expressing CtsZ were significantly larger than those that did not re-express CtsZ. (*C*) Representative images of CtsZ expression and macrophage (CD68^{+}) infiltration in tumors from RIP-*Tva*; *CtsZ*$^{-/-}$ RT2 mice injected with the RCAS-*CtsZ* virus, categorized according to whether or not tumors successfully re-expressed CtsZ. Bars: *left* and *middle* panels, 50 μm; *right* panel, 10 μm. (*D*) Ki67 staining was performed on tumors from RIP-*Tva*; *CtsZ*$^{-/-}$ RT2 mice injected with the RCAS-*CtsZ* virus that were categorized according to expression of CtsZ as in *C*. Quantification was performed and showed a significant increase in proliferation in tumors re-expressing CtsZ (n = 36 tumors negative for CtsZ expression; n = 18 tumors positive for CtsZ expression). (*E*) H&E staining was used to grade individual tumors from RIP-*Tva*; *CtsZ*$^{-/-}$ RT2 mice intracardially injected with the RCAS-*CtsZ* virus that were categorized as in *C*. The relative proportions of encapsulated (green), microinvasive (IC1; blue), and invasive (IC2; red) carcinomas were graphed. There is a significant increase in invasion of RIP-*Tva*; *CtsZ*$^{-/-}$ RT2 tumors re-expressing CtsZ compared with those that do not. Graphs in *B* and *C* show mean ± SEM. *P*-values in *B* and *D* were obtained using unpaired two-tailed Student's *t*-test, and *P*-values in *E* were obtained using a cumulative logit model; (n.s.) nonsignificant; (*) $P < 0.05$; (**) $P < 0.01$; (***) $P < 0.001$.

expression of the Tva receptor at the surface of cancer cells in vivo by immunofluorescence staining of RIP-*Tva*; *CtsZ*$^{-/-}$ RT2 tumors (Supplemental Fig. S3A). As expected, constitutive deletion of *CtsZ* in the RIP-*Tva*; RT2 model phenocopied the decrease in tumor burden observed in the *CtsZ*$^{-/-}$ RT2 mice (Fig. 4B). We next sought to determine the impact of cancer cell-specific expression of CtsZ by intracardially injecting RCAS-*CtsZ* virus into 7-wk-old RIP-*Tva*; *CtsZ*$^{-/-}$ RT2 animals (Fig. 4A). By performing immunostaining for CtsZ, we determined that ~30% of all tumors per mouse were successfully infected and re-expressed CtsZ specifically in cancer cells (Fig. 4C). We then compared the size of individual CtsZ-positive tumors with those tumors not re-expressing CtsZ present in the same animal and found that tumors that effectively re-expressed CtsZ were significantly larger than those that were not infected (Fig. 4B).

Accordingly, the proliferation rate was increased by 72% in CtsZ-re-expressing tumors in association with a 55% reduction in apoptosis, compared with tumors in which CtsZ expression was not restored (Fig. 4D; Supplemental Fig. S3B–D). Importantly, the introduction of the control GFP virus did not alter the tumor volume (Fig. 4B). These data, together with our BMT results, demonstrate that only cancer cell-intrinsic expression of CtsZ regulates RT2 tumor proliferation and growth. Moreover, histological analysis of tumor grade in RIP-*Tva*; *CtsZ*$^{-/-}$ RT2 mice injected with the RCAS-CtsZ virus revealed that tumors that effectively re-expressed CtsZ were significantly more invasive than those that were not infected with the virus (Fig. 4E). These results further underscore the dual role of tumor-supplied CtsZ in regulating both the proliferation and invasion of PanNETs.

Distinct regulation of the protumorigenic functions of CtsZ in cancer cells and macrophages

To determine the molecular mechanisms by which macrophage-derived and cancer cell-derived CtsZ differentially promote tumor progression and invasion, we used β-tumor cell (BTC) lines derived from wild-type or *CtsZ*$^{-/-}$ RT2 tumors and prepared BM-derived macrophages (BMDMs) from wild-type or *CtsZ*$^{-/-}$ mice for use in a panel of cell-based assays (Supplemental Fig. S4A). We first confirmed the absence of CtsZ mRNA expression, protein expression, and protein secretion in *CtsZ*$^{-/-}$ BTC lines and macrophages (Supplemental Fig. S4B–E). Similar analyses of other cathepsin family members showed no major alteration as a consequence of *CtsZ* deficiency in either cell type (Supplemental Fig. S4B–E), thus establishing that any effects observed in the cell culture assays are CtsZ-dependent. Deletion of *CtsZ* significantly reduced proliferation of tumor cells but not macrophages (Fig. 5A,B; Supplemental Fig. S5A,B). Moreover, the effect of *CtsZ* deletion on BTC proliferation was not rescued by addition of CtsZ to culture media through cancer cell-extrinsic sources, including exposure to wild-type macrophage conditioned medium (CM), or addition of exogenous recombinant CtsZ (Supplemental Fig. S5C). Together, the results obtained from our cell culture assays are consistent with the in vivo data above, demonstrating that the proliferative functions of CtsZ are cancer cell-intrinsic.

It has previously been shown that adhesive properties of endothelial cells (HUVECs [human umbilical vein endothelial cells]) are mediated by interaction of CtsZ and the extracellular domain of integrin β3 via the CtsZ RGD motif (Lechner et al. 2006). To address the role of CtsZ in cellular adhesion of tumor cells and macrophages to different matrices, we cultured each cell type on surfaces coated with collagen, Matrigel, or fibronectin and monitored their ability to attach in real-time using an xCELLigence live cell monitoring platform (Ke et al. 2011). We found that both macrophages and BTCs deficient for *CtsZ* showed impaired cell adhesion. However, the observed defects for each cell type were matrix-dependent. Interestingly, *CtsZ*$^{-/-}$ macrophage adhesion defects were restricted to fibronectin, while the attachment of *CtsZ*$^{-/-}$ BTCs was impaired for all matrices tested (Supplemental Fig. S5D,E). This suggests differences in integrin complex regulation in each cell type.

To investigate whether *CtsZ* deficiency also impeded the ability of both cell types to invade through ECM components, we examined invasion of *CtsZ*$^{-/-}$ BTCs and macrophages through transwells coated with a mix of Matrigel and collagen. *CtsZ*$^{-/-}$ macrophages and tumor cells were both defective in their invasive properties compared with wild-type controls (Fig. 5C,D), as we found for both cell types in vivo (Fig. 2E,F). This phenotype is unlikely to be dependent on extensive CtsZ-mediated ECM degradation, given that CtsZ is a carboxypeptidase with low processivity (Santamaria et al. 1998; Nagler et al. 1999; Kos et al. 2009). Rather, we propose that CtsZ-mediated invasion is likely due to nondegradative functions, which could be related to regulation of integrin-mediated cell adhesion and migration.

Integrin-dependent roles of CtsZ

To further examine whether and how CtsZ regulates integrin-dependent protumorigenic functions, we determined which integrins are present in the model systems used here and assessed whether their expression is altered by *CtsZ* deficiency. We performed qPCR analyses of a panel of integrin subunits that have been shown in previous studies to mediate attachment to the ECM matrices tested above (Humphries et al. 2006; Byron et al. 2010). These assays revealed no major changes in mRNA expression in wild-type or *CtsZ*$^{-/-}$ macrophages and cancer cells (Supplemental Fig. S6A) or in RT2 tumors deficient for the protease (Supplemental Fig. S6B).

Given that integrin expression was not altered in macrophages or BTCs in response to *CtsZ* deletion, we next wanted to test whether there were any differences in downstream intracellular signaling, indicative of possible integrin engagement. Indeed, through the recruitment and activation of signaling proteins such as nonreceptor

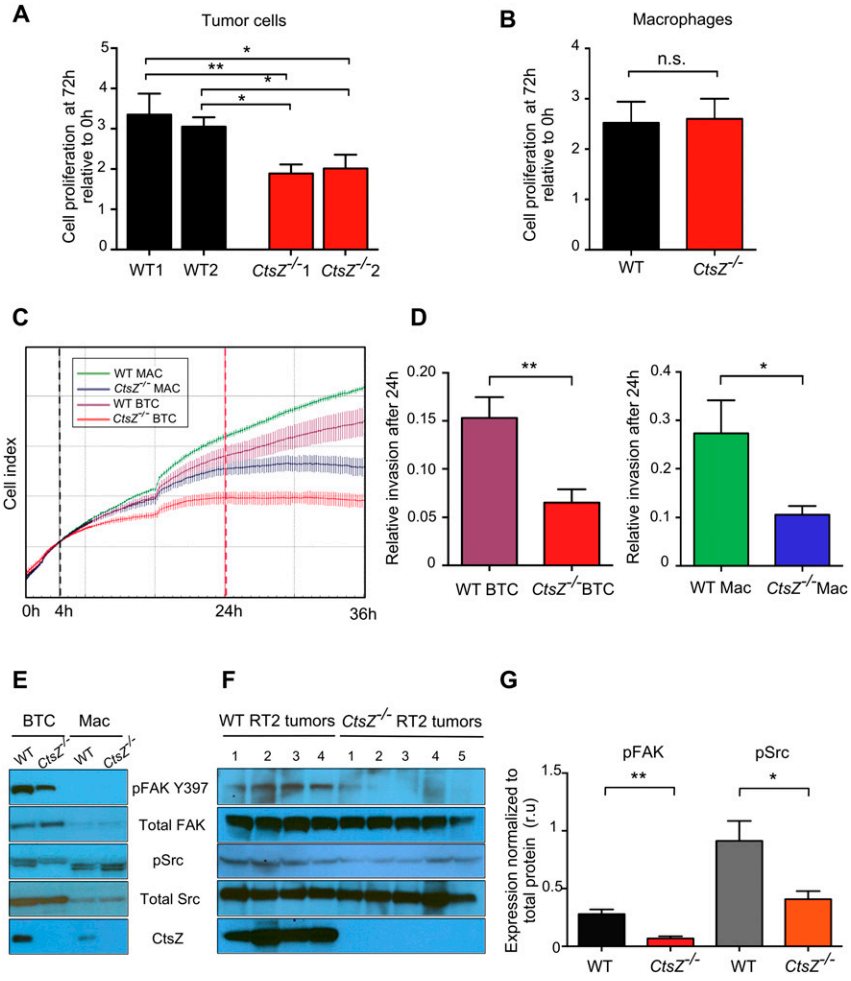

Figure 5. CtsZ differentially regulates tumorigenic properties of cancer cells and macrophages. Relative proliferation rates of wild-type (WT) and *CtsZ*$^{-/-}$ BTCs (two independent cell lines each) (*A*) and wild-type and *CtsZ*$^{-/-}$ macrophages (Mac) (*B*) were calculated every 24 h for 3 d by the MTT proliferation assay (see Supplemental Fig. S5A,B), and the 72-h endpoint is shown here. $n = 3$ replicate experiments. (*C*) Representative curves of in vitro invasion experiments monitored in real time using the xCELLigence system. (*D*) Invasion of BTCs and macrophages (suspended in serum-free medium) through a mix of Matrigel (1/30 dilution in serum-free medium containing 1 mg/mL collagen) toward regular medium (containing 10% FBS) using xCELLigence. $n = 6$ replicate experiments. Protein extracts from wild-type and *CtsZ*$^{-/-}$ BTC lines and macrophages grown on fibronectin-coated plates (*E*) and total extracts from whole wild-type RT2 or *CtsZ*$^{-/-}$ RT2 tumors (*F*) were analyzed for Src and FAK total protein and phosphorylated protein levels. (*G*) Quantification of pFAK and pSrc normalized to total FAK and total Src, respectively, using ImageJ software showed significant decreases in protein phosphorylation levels in *CtsZ*$^{-/-}$ RT2 compared with wild-type RT2 tumors. $n = 5$ replicate experiments. Graphs show mean ± SEM. *P*-values were obtained using unpaired two-tailed Student's *t*-test; (n.s.) nonsignificant; (*) $P < 0.05$ (**) $P < 0.01$.

tyrosine kinases, integrins can modulate multiple cellular processes, including motility, proliferation, and survival (Gabarra-Niecko et al. 2003; Desgrosellier and Cheresh 2010; Xiong et al. 2013). We therefore analyzed the activity of the downstream FAK–Src signaling pathway (Mitra and Schlaepfer 2006) in BTC lines, macrophages, and intact RT2 tumors lacking *CtsZ*. We found that phosphorylation of FAK and Src was significantly reduced in the absence of *CtsZ* in BTCs and in RT2 tumors (Fig. 5E–G). Phosphorylated FAK (pFAK) was not detectable in macrophages, and pSrc levels did not change in *CtsZ*$^{-/-}$ macrophages. The absence of FAK–Src modulation in response to *CtsZ* deletion in macrophages may also account for the observation that proliferation was not altered in this cell type.

Interestingly, treatment of wild-type BTCs with the Src inhibitor dasatinib (Nagaraj et al. 2010) or the selective FAK inhibitor PF-573228 (Slack-Davis et al. 2007) significantly reduced proliferation, while neither inhibitor had an effect on *CtsZ*$^{-/-}$ BTCs (Supplemental Fig. S6C–E). Together, these data suggest that integrin signaling is differentially modulated in response to *CtsZ* deletion in BTCs and macrophages. Furthermore, this cell type-specific difference is in accordance with our findings that CtsZ regulates adhesion and invasion of macrophages and cancer cells to different matrices, while the growth-promoting functions of CtsZ are restricted to cancer cells, potentially through differential regulation of the FAK–Src signaling pathway downstream from integrin activation.

We next sought to determine how intracellular CtsZ might interact with integrins to cause downstream activation of FAK–Src signaling in BTCs. Previous studies have shown that CtsZ-mediated catalytic cleavage of integrin β2 or RGD motif-dependent binding to integrin β3 can regulate both immune cell adhesion and migration (Lechner et al. 2006; Jevnikar et al. 2011). To uncouple the functions of the CtsZ catalytic site and the RGD motif in our experimental system, we infected *CtsZ*$^{-/-}$ BTCs with a doxycycline-inducible lentiviral pTRIPZ vector containing the full-length human *CtsZ* sequence (*hCtsZ*) or *hCtsZ* mutated for one or the other domain. Upon addition of doxycycline in cell culture, we confirmed that the BTC lines infected with each of the three different constructs efficiently expressed *hCtsZ*. qPCR analysis of *hCtsZ* mRNA and the other endogenously detectable cathepsins and immunoblots using a hCtsZ antibody showed comparable expression levels between

the different genetically manipulated BTC lines (Supplemental Fig. S7A,B).

We first investigated the impact of these constructs on cell proliferation. As expected, expression of full-length CtsZ (+CtsZ) in *CtsZ*$^{-/-}$ BTCs restored the proliferation index to the level of wild-type BTCs. Similar results were obtained when the *CtsZ* construct mutated at the catalytic site (+CtsZ-catsite^{mut}) was introduced into *CtsZ*$^{-/-}$ BTCs. However, expression of the *CtsZ* construct that was mutated in the RGD motif (+CtsZ-RGD^{mut}) was unable to rescue proliferation (Fig. 6A). We then evaluated the invasive properties of the *CtsZ* mutants in real time using the xCELLigence platform, as described above. In this assay, only *CtsZ* mutated in the RGD motif displayed a significant defect in invasion, comparable with *CtsZ* deletion (Fig. 6B). We next sought to determine whether the proliferative advantage conferred by the CtsZ RGD motif was associated with regulation of the FAK–Src pathway in BTCs. Analyses of pFAK and pSrc levels in *CtsZ* mutant BTC lines revealed a defect in activation of these proteins specifically when the RGD motif of CtsZ was mutated, while the catalytic site mutation restored pathway activity (Fig. 6C,D). Together, these results indicate that the proproliferative and proinvasive functions of cancer cell-derived CtsZ are predominantly regulated through its RGD domain.

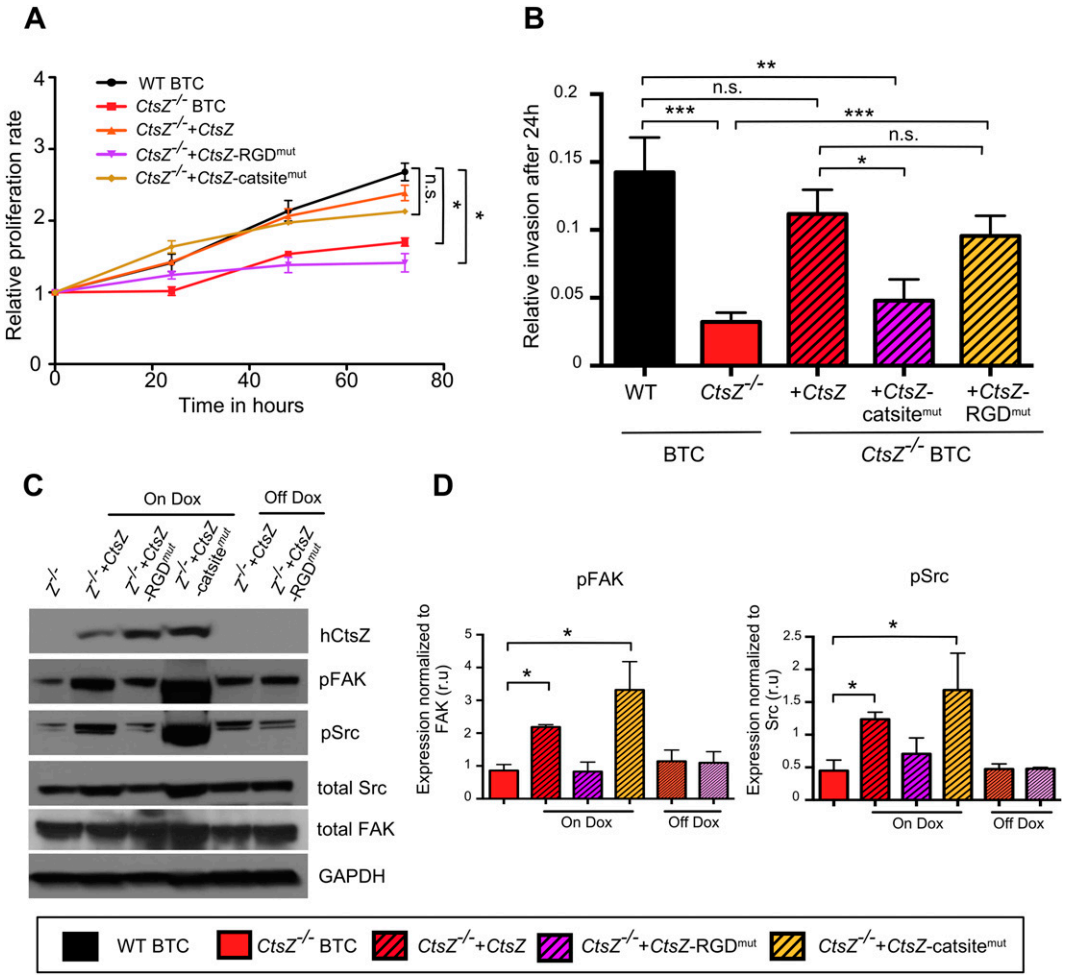

Figure 6. The CtsZ RGD motif is critical for cancer cell growth and invasion and modulates FAK and Src activity. (*A*) Relative proliferation rates of wild-type (WT) BTC, *CtsZ*$^{-/-}$ BTC, or *CtsZ*$^{-/-}$ BTC lines infected with a lentivirus containing either the full-length human *CtsZ* mRNA or *CtsZ* mutated for the RGD domain or the catalytic site (catsite) (collectively referred to here as experimentally manipulated *CtsZ*$^{-/-}$ BTCs) (see the Materials and Methods for details). Proliferation was monitored every 24 h for 3 d by the MTT assay. (*B*) Invasion of wild-type BTCs, *CtsZ*$^{-/-}$ BTCs, or the different manipulated *CtsZ*$^{-/-}$ BTCs through a mix of Matrigel and collagen (as in Fig. 5) in response to regular medium (10% FBS) was monitored using xCELLigence. (*C*) Protein extracts from *CtsZ*$^{-/-}$ BTCs and manipulated *CtsZ*$^{-/-}$ BTCs were analyzed for FAK and Src expression and phosphorylation. Re-expression of the full-length or catalytic mutant *CtsZ* caused increased phosphorylation of both FAK and Src compared with *CtsZ*$^{-/-}$ BTCs, while re-expression of RGD mutated *CtsZ* did not. (*D*) Quantification of pFAK and pSrc normalized to total FAK and total Src, respectively, using ImageJ software showed no increase in protein phosphorylation in RGD mutated BTCs. $n = 3$ replicate experiments. Graphs show mean ± SEM. *P*-values were obtained using unpaired two-tailed Student's *t*-test; (n.s.) nonsignificant; (*) $P < 0.05$ (**) $P < 0.01$ (***) $P < 0.001$.

Interplay between cancer cell-derived and TAM-derived CtsZ in tumor invasion

The BMT experiments showed that macrophage-supplied CtsZ supports the invasion of cancer cells in vivo. We hypothesized that TAMs might assist cancer cell invasion by intercellular transfer of secreted CtsZ onto the cell surface of tumor cells, possibly by binding to integrins, as previously suggested in other contexts (Lechner et al. 2006; Lines et al. 2012). To test this hypothesis, we analyzed the activity profile of CtsZ on the surface of wild-type or $CtsZ^{-/-}$ BTCs in culture when exposed to CM from wild-type or $CtsZ^{-/-}$ macrophages. We performed cell surface labeling of CtsZ with the membrane-impermeable cathepsin activity-based probe (ABP) DCG-04 (Greenbaum et al. 2000) prior to pull-down purification of ABP-reactive polypeptides using streptavidin-agarose beads. ABP labeling was performed at 4°C to suppress all membrane dynamics and cellular trafficking. Immunoblotting of the purified material using a CtsZ-specific antibody revealed an increase in active CtsZ at the surface of BTCs when exposed to wild-type macrophage CM compared with $CtsZ^{-/-}$ macrophage CM (Fig. 7A). The increase in cell surface CtsZ activity was more pronounced in wild-type BTCs compared with $CtsZ^{-/-}$ BTCs (Fig. 7A), consistent with a portion of the CtsZ cell surface fraction also being secreted by tumor cells in addition to binding of macrophage-derived CtsZ. CtsB was used as a control in these experiments and showed minimal changes in activity-based labeling under the different conditions tested (Fig. 7A).

We additionally performed immunostaining of CtsZ in cultures of wild-type or $CtsZ^{-/-}$ BTCs exposed to CM from wild-type or $CtsZ^{-/-}$ macrophages under minimal cell permeant conditions. This was followed by quantitation of cancer cells positive for CtsZ on the cell surface. Interestingly, we observed that stimulation with wild-type macrophage CM led to a 2.9-fold increase in the number of wild-type BTCs showing cell surface-associated CtsZ (Fig. 7B,C). There was no such increase when $CtsZ^{-/-}$ macrophage CM was applied. Analysis of $CtsZ^{-/-}$ BTCs also revealed an increase in CtsZ levels at the cell surface when wild-type macrophage CM was added, although the baseline levels of CtsZ were considerably lower than in wild-type BTCs, consistent with the ABP-labeling results above. Interestingly, macrophage-derived CtsZ was not substantially internalized into $CtsZ^{-/-}$ cancer cells, potentially explaining why exogenous CtsZ did not

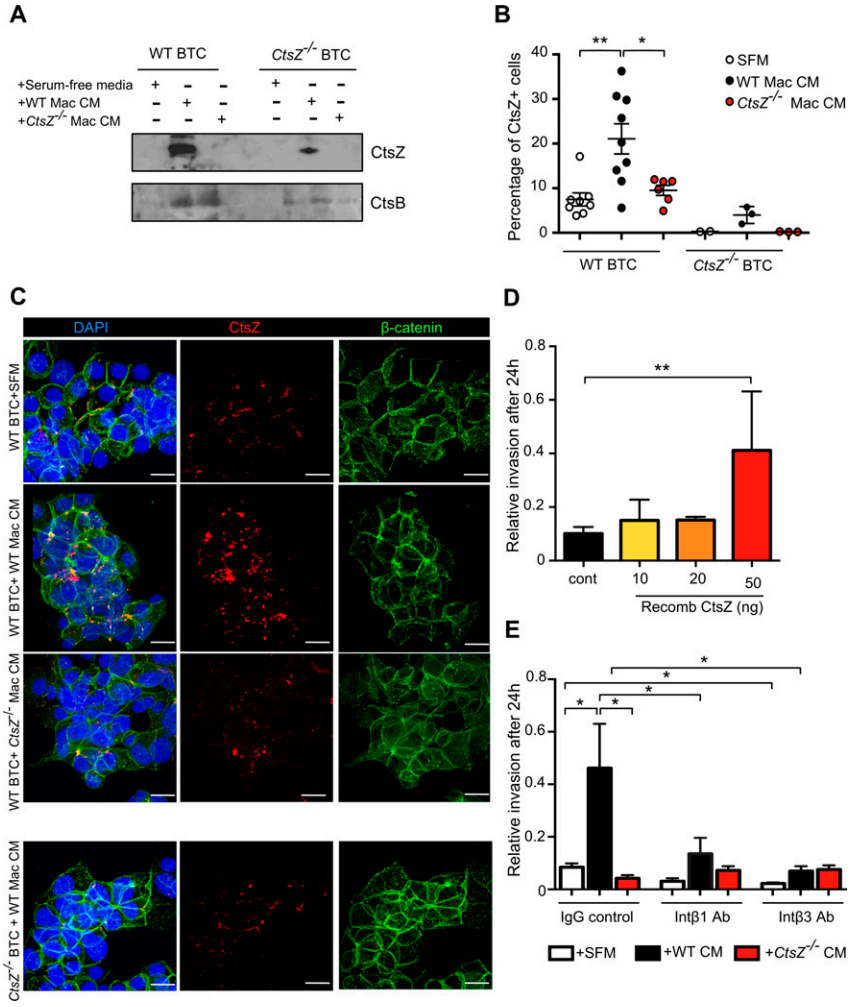

Figure 7. Macrophage-derived CtsZ binds to cancer cells to enhance integrin-dependent invasion. (*A*) Cell surface expression and activity of CtsZ on wild-type (WT) and $CtsZ^{-/-}$ cancer cells. Wild-type and $CtsZ^{-/-}$ BTCs were exposed for 24 h to serum-free medium, wild-type macrophage CM, or $CtsZ^{-/-}$ macrophage CM prior to extensive washing and incubation with the cathepsin ABP DCG-04 (10 μmol/L) for 1 h at 4°C followed by additional PBS washes. Western blots of cell lysates using CtsZ- and CtsB-specific antibodies were developed with streptavidin peroxidase after performing pull-down purification of DCG-04-reactive polypeptides using streptavidin-agarose beads. Representative blots of three independent experiments are shown. (*B*,*C*) Wild-type and $CtsZ^{-/-}$ BTCs were grown and stimulated as described above prior to ice-cold ethanol fixation followed by cell surface staining of CtsZ. (*B*) Quantitation of CtsZ staining. (*C*) Representative images. Bars: all panels, 20 μm. (*D*) Invasion of wild-type BTCs stimulated with increasing concentrations of recombinant CtsZ was performed and monitored using xCELLigence. (*E*) Invasion of wild-type BTCs stimulated with either wild-type or $CtsZ^{-/-}$ macrophage CM in the presence of control IgG or blocking antibodies against integrins β1 or β3 was quantified using xCELLigence. (SFM) Serum-free medium. n = 4–6 replicate experiments. Graphs show mean ± SEM. P-values were obtained using unpaired two-tailed Student's t-test; (*) $P < 0.05$; (**) $P < 0.01$.

have any effect on cancer cell proliferation. Taken together, these results support our hypothesis that macrophages promote cancer cell invasion through cell surface binding of secreted CtsZ.

We further tested this hypothesis by analyzing cancer cell invasion following stimulation with increasing concentrations of recombinant CtsZ (which contains the propeptide) in the cell culture medium. We observed enhanced invasion of BTCs, suggesting that exogenous CtsZ indeed promotes invasion of cancer cells (Fig. 7D). In order to determine whether macrophage-derived CtsZ similarly enhanced cancer cell invasion, we exposed wild-type BTCs to wild-type or *CtsZ*$^{-/-}$ macrophage CM 2 h prior to performing invasion assays (Fig. 7E). Invasion was significantly enhanced only when BTCs were exposed to wild-type macrophage CM, consistent with our in vivo results showing that TAM-derived CtsZ promotes cancer cell invasion.

Given our findings above that the RGD motif of CtsZ is a critical regulator of its proinvasive functions, we asked whether the proinvasive properties of macrophage-derived CtsZ were mediated via binding to integrins at the cancer cell surface. Cancer cells were stimulated by wild-type or *CtsZ*$^{-/-}$ macrophage CM in the presence of blocking antibodies against integrin β1 (Sangaletti et al. 2008) or integrin β3 (Ashkar et al. 2000). Neutralizing either of these integrins led to inhibition of the proinvasive effects provided specifically by wild-type macrophage CM. Interestingly, at the basal level, BTC invasion was also inhibited by integrin β3 blockade (Fig. 7E). We further examined whether neutralizing these integrins has an effect on cancer cell proliferation. While inhibition of integrin β3 had a modest effect on cell growth, we observed no significant alteration in response to integrin β1 blockade (Supplemental Fig. S7C). Together, these results demonstrate that blocking the RGD-dependent interactions of CtsZ with integrin receptors is sufficient to impair cancer cell invasion, thus emphasizing the importance of the RGD motif for the proinvasive function of CtsZ independent of its catalytic activity.

Discussion

While several members of the cathepsin family have been identified as major players in tumorigenesis, based on significant associations between increased expression levels and negative patient prognosis in many tumor types and the effects of cathepsin deletion or inhibition in various mouse models of cancer (Mohamed and Sloane 2006; Palermo and Joyce 2008), far less is known about the potential roles of CtsZ in cancer. High CtsZ expression correlates with advanced malignancy in hepatocellular carcinomas and colorectal and prostate cancer (Hidaka et al. 2000; Nagler et al. 2004; Wang et al. 2011; Vizin et al. 2012). Interestingly, CtsZ is also up-regulated in the inflammatory condition of *Helicobacter pylori*-associated gastritis, further increased in gastric cancer, and induced in both infiltrating macrophages and epithelial cells (Krueger et al. 2005; Bernhardt et al. 2010). Therefore, it will be intriguing to now determine whether CtsZ plays roles in these diverse tumor microenvironments similar to those that we uncovered for pancreatic neuroendocrine cancers.

Here, we identify a critical role of CtsZ in promoting PanNET development by regulating cancer cell proliferation and invasion. Intriguingly, we found that key tumorigenic functions of this cathepsin are mediated via the RGD motif in the prodomain of CtsZ, while its catalytic activity was not required for regulation of either proliferation or invasion of cancer cells. In contrast to the dual effect of CtsZ on proliferation and invasion of cancer cells, only invasion was impaired in the absence of CtsZ in macrophages. These results suggest that while the RGD motif of CtsZ is critical for its tumor-promoting functions, it acts differently in each cell type. One possible explanation is differences in subcellular localization of CtsZ that lead to activation of downstream signaling pathways in a different manner in cancer cells compared with macrophages. Indeed, we found that the FAK–Src signaling pathway, which is classically associated with formation of focal adhesion complexes in response to integrin engagement, is specifically impaired in cancer cells and not macrophages following constitutive deletion of *CtsZ* or mutation of the *CtsZ* RGD motif. It has previously been suggested that, in addition to the RGD-dependent extracellular binding of CtsZ to integrin β3, CtsZ traffics from intracellular compartments to accumulate in vesicles at the cell membrane prior to secretion and that this phenomenon is also dependent on its RGD motif (Lechner et al. 2006). Therefore, differences in secretory pathways between cancer cells and macrophages might explain the extended presence of CtsZ juxtaposed to the cell membrane at the intracellular surface, resulting in activation of the FAK–Src pathway specifically in cancer cells, thus contributing to its proliferative functions.

These results are supported by the inability of macrophage-derived CtsZ to promote cancer cell proliferation in vitro or rescue tumor proliferation in vivo in the BMT experiments. Our data also indicate that macrophage-derived CtsZ is not substantially internalized into *CtsZ*$^{-/-}$ cancer cells, potentially explaining the specificity of the intracellular effects of CtsZ on proliferation. Therefore we conclude that the proproliferative functions of CtsZ are exclusively cancer cell-intrinsic. Intriguingly, we also found that FAK or Src inhibitors only reduce cell proliferation in BTC lines expressing CtsZ. This result suggests a key role for CtsZ in mediating the proliferative effects of FAK and Src signaling in PanNET cells, which will also be interesting to investigate in other cancer types.

In contrast, the effects of CtsZ on cancer cell invasion are in part derived by macrophage-supplied CtsZ, and cell surface analysis of CtsZ demonstrated the increased presence and activity of the protease on the surface of cancer cells when exposed to macrophage CM. Using blocking antibodies against specific integrins (β1 and β3) known to colocalize with CtsZ, we demonstrated that invasion is significantly diminished by inhibiting the capacity of integrin complexes at the cell surface to interact with CtsZ. Interestingly, cancer cell-derived

CtsZ is predominantly secreted in the active form that lacks the RGD motif, whereas macrophage-derived CtsZ is also secreted as the proform. Thus the ability of macrophage-derived CtsZ to preferentially associate with the cancer cell surface via integrin binding is one possible explanation for how it enhances invasion.

We show here that CtsZ promotes invasion and migration via a noncatalytic mechanism, which contrasts with the proteolytic roles of other proinvasive cathepsin family members (Fonovic and Turk 2014; Sevenich and Joyce 2014), including those previously analyzed in the RT2 model (Gocheva et al. 2006, 2010b). This suggests that multiple modes of cell invasion may be important in PanNET malignancy and likely other tumor types. For instance, it is possible that CtsZ-driven mechanisms could modulate migration and invasion at the single-cell level by engaging integrins in response to changes in the ECM, while collective invasion could be promoted by a switch to CtsB/L/S-driven dissolution of cell–cell junctions and ECM degradation (Fig. 8). The ability of cancers to alternate between these different mechanisms of cell invasion would thus provide the tumor with the maximum flexibility to invade through matrices of different composition and stiffness (Friedl and Wolf 2010; Friedl et al. 2012). In sum, this study identified a novel mechanism of heterotypic cell signaling within the tumor microenvironment that centers on CtsZ (Fig. 8), resulting in the promotion of cancer malignancy.

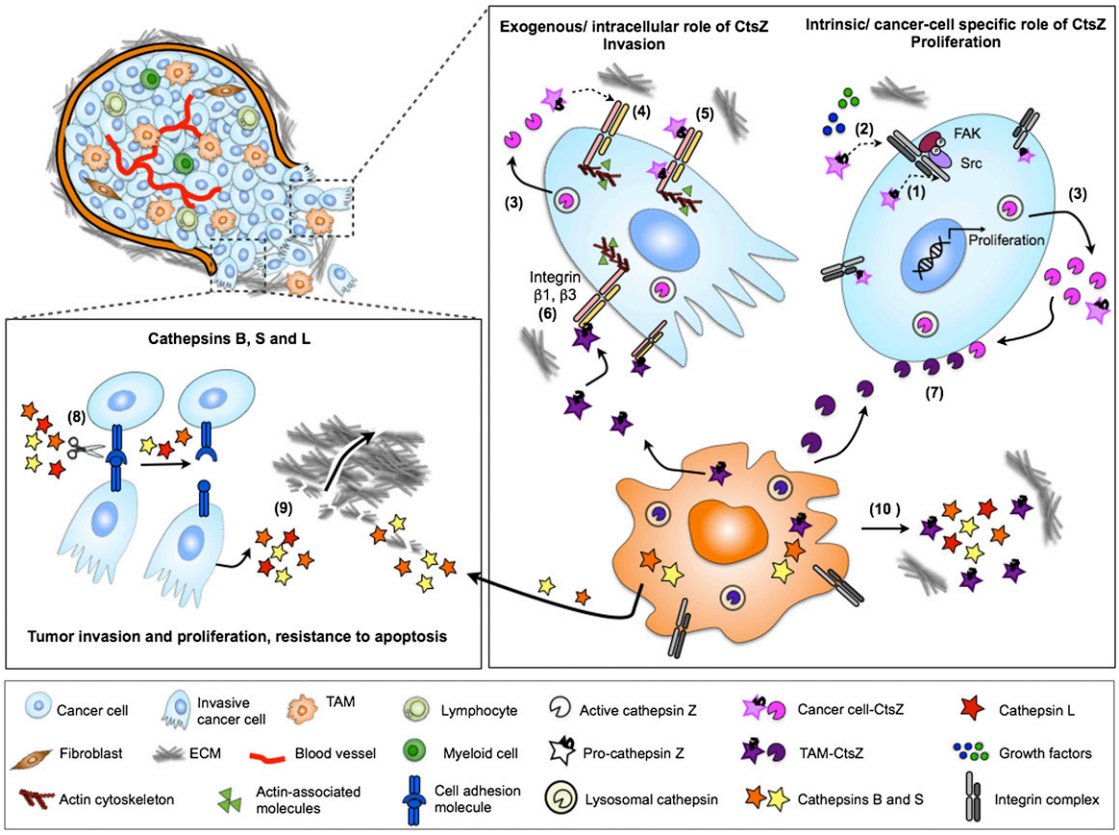

Figure 8. Model depicting CtsZ regulation of the protumorigenic functions of TAMs and cancer cells. Cancer cell-derived CtsZ regulates intracellular proliferation through the RGD motif located in the prodomain via activation of the FAK/Src signaling pathway. This process can occur through enhancing growth factor/adhesion-dependent integrin complex signaling either by intracellular regulation of the C-terminal tail of β-chain integrins by CtsZ (1) or at the cell surface through direct and/or indirect interaction with integrin complexes (2). (3) CtsZ is secreted by cancer cells mainly as an active enzyme and is detected in its active form at the cancer cell surface. While we found that active CtsZ is not necessary for the invasive properties of CtsZ, it could potentially enhance motility. (4,5) Although less substantially produced than the active form, tumor cell-derived pro-CtsZ can also enhance invasion by inducing the outside-in signaling of integrins, leading to focal adhesion complexes and actin cytoskeleton remodeling, depending on integrin complexes involving the β1 or β3 chains. In a complementary manner, intracellular functions of CtsZ on integrin complexes could also promote cell motility by regulating the inside-out integrin pathway. (6) Critically, TAM-derived CtsZ is secreted as both a proform and an active form of the enzyme and binds to the cancer cell surface to promote integrin β1- and β3-dependent cancer cell invasion. (7) CtsZ derived from TAMs leads to enhanced levels of active CtsZ at the cancer cell surface, although it is not substantially internalized and does not promote proliferation. (8) In addition to CtsZ-mediated regulation of cancer cell invasion, CtsB, CtsL and CtsS cleave intercellular adhesion molecules as E-cadherin and JAMs, thereby enhancing migration (Gocheva et al. 2006; Sevenich et al. 2014). (9) Degradation of ECM components by these cathepsins leads to enhanced cancer cell invasion and tumor malignancy. (10) TAMs express and secrete high levels of CtsB, CtsS and CtsZ, all of which contribute to promoting tumor progression (Gocheva et al. 2010b); however, only CtsZ regulates the migratory and invasive properties of TAMs in vivo, as we show here.

Materials and methods

Mouse strains

The generation and characterization of RT2 and *CtsZ*$^{-/-}$ mice (mutant *Ctsz* allele, referred to here as *CtsZ*) have been previously reported (Hanahan 1985; Sevenich et al. 2010). *CtsZ* heterozygous mice were backcrossed into the C57BL/6 background for nine generations before crossing to RT2 mice. The RIP-*Tva* mice (Du et al. 2007) were a kind gift of Dr. Nancy Du and Dr. Harold Varmus and were crossed with RT2 mice to generate RIP-Tag; RIP-*Tva* mice in a wild-type or *CtsZ*$^{-/-}$ background. β-Actin GFP transgenic mice (Okabe et al. 1997) in the C57BL/6 background were purchased from Jackson Laboratories. All animal studies were performed using protocols approved by the institutional animal care committee at Memorial Sloan-Kettering Cancer Center (MSKCC).

TMA construction

A TMA was constructed from archival paraffin-embedded tissue from a series of 80 PanNETs surgically resected from patients at MSKCC. Patient anonymity was ensured, and the study was performed in compliance with the institutional review board. The pancreatic tumors used in the array included the following: 11 insulinomas, 63 pancreatic endocrine tumors (with islet cell tumors representing the majority), and six metastases from pancreatic endocrine neoplasms. Specimens of normal pancreas ($n = 6$) were also included in the TMA. Three 0.6-mm tissue cores were punched from representative areas of the donor block and embedded in a recipient block using an automated TMA machine. The TMA block was sectioned (5 μm thick), and the slides were stained for hCtsH and hCtsZ (R&D Systems). The cathepsin staining for each tissue specimen was scored in a blinded manner (by J.A. Joyce) as negative (0), weakly positive (1), moderately positive (2), or strongly positive (3) and graphed as the percentage of staining intensity for each stage: normal pancreas, benign tumor, vascular invasive tumor, invasive tumor, metastatic primary tumor, and metastasis (to liver or lymph nodes). Benign tumors were classified as lesions in which there was no evidence of either tumor or vascular invasion (benign, $n = 22$). Vascular invasive tumors were classified by the presence of tumor cells or tumor emboli in the blood or lymphatic vasculature (vascular invasive, $n = 12$). Invasive tumors were classified into two groups: those showing either frank tumor cell invasion but no evidence of metastases (invasive tumor, $n = 11$) or those in which the primary PET lesion had metastasized to a secondary organ (metastatic primary, $n = 23$). Metastases to the liver and/or lymph nodes were also scored (metastasis, $n = 6$). For each cathepsin (Z and H), an overall test of differences among any of the groups (normal and tumor) was performed. An exact version of Mantel Haenszel's test for trend was performed to look for differences in staining in each tumor group compared with the normal controls. Since multiple comparisons were performed, a P-value of <0.01 was considered significant.

Tissue collection and analysis

For analysis of angiogenic switching, RT2 mice were sacrificed at 10.5 wk of age by heart perfusion with 10 mL of PBS under proper anesthesia. The pancreas was then removed and minced gently with scissors. The number of angiogenic islets, distinguishable by their red and hemorrhagic appearance, were counted under a dissecting microscope. The average of the sum of all angiogenic islets per mouse was compared between the different genotypes.

Tumor volume and number were determined in all experiments at 13.5 wk of age, and RT2 mice were sacrificed by heart perfusion with PBS followed by 10% zinc-buffered formalin. Tumor-containing pancreas and control tissues were removed, placed in 30% sucrose overnight, and embedded in OCT (Tissue-Tek). The dimensions of the tumors were measured with a ruler, and their volume was calculated using the formula volume = width^2 × length × 0.52 to approximate the volume of a spheroid. Tumor burden was represented as the sum of the volumes of all tumors per mouse.

Histological analysis

For the phenotypic characterization of wild-type and *CtsZ*$^{-/-}$ RT2 tumors, frozen 10-μm-thick sections were cut on a cryostat and analyzed by immunostaining. The CtsZ expression pattern was analyzed by immunofluorescence. Briefly, frozen sections from wild-type RT2 animals were dried for 30 min at room temperature, rehydrated in PBS for 10 min, and preincubated with 1× PNB blocking buffer (PerkinElmer Life Sciences) for 1 h and incubated with the primary antibody of interest overnight at 4°C (diluted in 1× PNB). Antibodies against the following were used: CD45, CD31, CD4, and CD8 (BD Pharmingen); CtsZ (R&D Systems); CD68, F4/80, and 7/4 (Serotec); NG2 (Chemicon); GFP (Invitrogen); SYP (Dako); and Iba1 (Wako). The Tva antibody (rabbit) was a kind gift of Dr. Andrew Leavitt (University of California at San Francisco). All antibody information—including species, clone, and optimized concentration—is shown in Supplemental Table 3. Paraffin sections of human samples stained for SYP and CD68 (Fig. 1, as shown in D and quantified in E) were processed using a Ventana automated staining device. The automated rehydration, citrate buffer-based antigen retrieval, and blocking of unspecific protein binding was followed by incubation with SYP or CD68 primary antibodies and the CtsZ antibody overnight at 4°C. The corresponding secondary antibodies were used at a 1:500 dilution and incubated for 1 h at room temperature. DAPI (1:5000; Invitrogen) was used to label the cell nuclei, and the slides were mounted in ProLong Gold mounting medium (Invitrogen). The tissues were observed under a Carl Zeiss Axioimager Z1 microscope, and images were acquired with Axiovision software using an Apotome (Zeiss) or with TissueFAXS software (TissueGnostics).

For analysis of human samples, 10–12 fields of view per sample were acquired using a 20× objective (total magnification, 200×) and a Zeiss Apotome to ensure cells were in the same optical section. The number of SYP$^+$ cancer cells and CD68$^+$ macrophages and the relative CtsZ intensity (CtsZ index) were evaluated using CellProfiler 2.0 software. A CellProfiler module was generated that allowed for the detection of cancer cells and macrophages based on their DAPI and SYP signal or DAPI and CD68 signal, respectively. The CtsZ signal intensity was measured in the whole-cell population (DAPI$^+$) and associated with a specific cell type (macrophages or cancer cells), and the proportion of CtsZ signal associated with SYP$^+$ cancer cells or CD68$^+$ macrophages was calculated relative to the overall CtsZ signal intensity in all DAPI$^+$ cells.

To analyze proliferation rates in tumors, sections were stained with a rabbit anti-mouse Ki67 antibody (Vector Laboratories), and the numbers of Ki67$^+$ cells relative to total cell number were determined using TissueQuest software. For apoptosis analysis, frozen sections were stained using rabbit anti-mouse CC3 (Cell Signaling Technology). The number of CC3$^+$ cells was counted using TissueQuest software, and the percentage of cell death was calculated as the percentage of the total cells per tumor. For invasion grading, hematoxylin and eosin (H&E) staining was performed, and the lesions were graded as previously described

(Lopez and Hanahan 2002) following a double-blind protocol and were independently assessed by two investigators (L. Akkari,/V. Gocheva/J.C. Kester and J.A. Joyce). The numbers of tumors and mice analyzed are specified in the figure legends. For the angiogenesis analysis, tumor sections from 13.5-wk-old wild-type or *CtsZ*$^{-/-}$ RT2 mice were stained with a rat anti-CD31 antibody, and the vessel area was calculated as the ratio of CD31^{+} endothelial cells divided by the DAPI^{+} tumor area as detected by pixel intensity and analyzed using Metamorph imaging software.

BMT protocol

BM was harvested from wild-type or *CtsZ*$^{-/-}$ β-actin-GFP mice by flushing the femurs and tibias with X-VIVO 20 medium (Cambrex) under sterile conditions. The flushed cells were resuspended in PBS, and 1×10^6 nucleated cells were injected into the tail veins of 4-wk-old wild-type or *CtsZ*$^{-/-}$ RT2 animals, which were lethally irradiated (950 rads) 6–8 h prior to injection. After 4 wk, recipient mice were bled from the orbital sinus to evaluate BM transplantation efficiency by determining the percentage of GFP^{+} cells using flow cytometry (80.6% GFP^{+} cells for wild-type; 83.7% GFP^{+} cells for *CtsZ*-deficient animals). Mice were subsequently aged to 13.5 wk for calculation of tumor volume and analysis of the tumor phenotype.

RCAS-Tva somatic gene transfer experiments

Viral propagation and delivery of the RCAS viruses were performed as described previously (Du et al. 2007). Briefly, DF-1 chicken fibroblasts (Himly et al. 1998) transfected with RCASBP vectors containing the GFP control sequence or the mouse *CtsZ* cDNA sequence were maintained in DMEM supplemented with 10% FBS and 1% penicillin/streptomycin in a humidified 37°C incubator under 5% CO_2. For in vivo infection, viral supernatant from the infected DF-1 cells was passed through 0.45-μm filters and concentrated by high-speed ultracentrifugation at 23,000 rpm for 1.5 h before intracardiac injection of 100 μL into mice. Intracardiac injection was performed as described previously (Kang et al. 2005).

Flow cytometry and sorting

Tumors from RT2 mice were isolated and processed for FACS analysis or sorting as described previously (Song et al. 2005).

RNA isolation, cDNA synthesis, and quantitative real-time PCR

RNA was isolated with Trizol and DNase-treated, and 0.2 μg of RNA was used for cDNA synthesis. Details about the individual TaqMan assays can be found in Supplemental Table 2. Gene expression was determined relative to expression of the housekeeping gene *Ubc* or *Hprt* in all qPCR experiments.

Generation of CtsZ manipulated BTC lines

The *hCtsZ* cDNA was purchased in a TrueClone vector (Origene) and cloned into the pBluescript II KS vector (Stratagene). Site-directed mutagenesis (QuickChange II; Stratagene) was used to mutate codon 38 from CGG (R) to CAC (H) or codon 92 from TGC (C) to AGC (S), thereby changing the CtsZ RGD motif to HGD or the active site cysteine to serine, respectively. Subsequently, the wild-type *CtsZ* and the two mutant variants were amplified by PCR with primers generating restriction sites for AgeI and MluI at the ends of the PCR product. Using these sites, the purified PCR products were cloned into the doxycycline-inducible lentiviral pTRIPZ shRNAmir vector (Thermo Fisher Scientific) in which the shRNAmir site and the red fluorescent protein reporter were replaced by the *CtsZ* cDNA. DNA sequencing confirmed the correct insertion and integrity of the cDNAs as well as presence of the intended *CtsZ* mutations. Lentiviral vectors were transfected into 293T cells with Lipofectamine (Life Technologies), according to the manufacturer's instructions. Supernatants were used to infect BTCs. Puromycin (2 μg/mL) was used as the selection agent.

Proliferation assays

Three independent wild-type and two *CtsZ*$^{-/-}$ BTC lines were derived from individual RT2 tumors using previously described methods (Efrat et al. 1988). BMDMs were prepared as previously described (Pyonteck et al. 2013). Cell growth rate was determined using an MTT cell proliferation kit (Roche). Briefly, cells were plated in triplicate in 96-well plates (2.5×10^3 for wild-type and *CtsZ*$^{-/-}$ mutant BTCs and 5×10^3 for macrophages from either genotype) on either plastic (Fig. 5A; Supplemental Fig. S5A,B) or a coating of 20 μg/mL fibronectin (Fig. 6A; Supplemental Figs. S6C,D, S7C). When indicated, BTCs were exposed to 50 nM dasatinib or PF-573228. Reduction of the MTT substrate was detected by colorimetric analysis using a plate reader as per the manufacturer's recommended protocol. Ten microliters of MTT labeling reagent was added to each well and then incubated for 4 h at 37°C followed by the addition of 100 μL of MTT solubilization reagent overnight. The mixture was gently resuspended, and absorbance was measured at 595 nm and 750 nm on a spectraMax 340pc plate reader (Molecular Devices). Data are shown relative to MTT values obtained at the start point of 0 h.

Adhesion and invasion assays

Real-time cell analyses (RTCAs) of macrophages and tumor cell adhesion and invasion were performed using the xCELLigence DP apparatus (Roche Diagnostics) as described in the manufacturer's instruction manual. Measurements of changes in impedance reflecting adhesion or invasion dynamics were determined using E-Plates (a single-chamber device) (Ke et al. 2011) or CIM-Plates (a two-chamber device separated by a porous membrane) (Limame et al. 2012), respectively, and were performed under sterile conditions and incubated at 37°C in 5% CO_2. Briefly, cells were trypsinized with 0.05% Trypsin/0.02% EDTA solution for 1–2 min at 37°C, and the reaction was stopped by the addition of 10% FBS-containing medium (DMEM + 1% penicillin/streptomycin; Gibco). Subsequently, 4×10^4 cells were resuspended in 100 μL of 10% FBS-containing medium and added to the E-Plate wells that were either uncoated or coated with 50 μg/mL collagen, 1% Matrigel, or 100 μg/mL fibronectin when performing adhesion assays. For invasion experiments, 5×10^4 cells per well, resuspended in 100 μL of serum-free medium, were added to the upper chamber of a CIM-Plate coated with 30 μL of a mix of Matrigel and collagen I (Matrigel diluted 1/30 in serum-free medium and 1 mg/mL rat tail collagen; BD Biosciences) prior to cell seeding. To induce cell invasion, the lower chamber of the CIM-Plate contained 10% FBS. In the indicated experiments, 10, 20, or 50 ng/mL recombinant CtsZ or CM from wild-type or *CtsZ*$^{-/-}$ macrophages was added to the upper chamber after stimulation of BTCs for 2 h under the indicated conditions. Recombinant CtsZ (R&D Systems) contained the RGD-binding site in the prodomain. Cell indices were measured every 15 min for up to 12 h for adhesion assays and 24 h for invasion assays with the RTCA software (version 1.2, Roche Diagnostics). Relative invasion and adhesion were determined by calculation

of slopes from the normalized cell indices of the adhesion or invasion curves (normalization was performed at 15 min for adhesion and 4 h for invasion) at the indicated time points (4 h or 8 h for adhesion and 24 h for invasion).

CM preparation, protein isolation, and Western blotting

CM from wild-type or *CtsZ*$^{-/-}$ BTCs or macrophages was generated by incubating confluent cell layers in serum-free DMEM for 24 h. Collected CM was centrifuged and passed through 0.22-μm filters to remove debris. For Western blotting, CM was concentrated by centrifugation in centrifugal filter units (Millipore). For protein isolation from cells grown in monolayer, cells were harvested by scraping and lysed in RIPA lysis buffer (Pierce) with 1× complete mini protease inhibitor cocktail (Roche). For protein isolation from whole tumors, snap-frozen samples were homogenized in RIPA lysis buffer (Pierce) with 1× complete mini protease inhibitor cocktail (Roche) followed by dounce homogenization. Protein was quantified using the BCA assay (Pierce). Protein lysates were loaded onto SDS-PAGE gels and transferred to PVDF membranes for immunoblotting. Membranes were probed with antibodies as indicated in Supplemental Table 3 and detected using the appropriate HRP-conjugated secondary antibodies using chemoluminescence detection (Millipore). Bands from Western blots were quantified in the dynamic range using the gel analysis module in ImageJ software.

Cell surface labeling of active CtsZ

Cell surface labeling of cysteine proteases using the biotinylated ABP DCG-04 (10 μM, 1 h at 4°C) (Greenbaum et al. 2000) was performed as described previously (Vasiljeva et al. 2006). DCG-04 was synthesized at the Organic Synthesis core facility at MSKCC. Briefly, cells were grown to confluency prior to medium removal and incubated for 1 h at 4°C with ice-cold medium containing 50 mmol/L HEPES and 10 μmol/L DCG-04. Cells were thoroughly washed and harvested by scraping and lysed on ice in 250 mmol/L Tris-HCl (pH 6.8) and 0.1% Triton X-100 containing 10 mmol/L EDTA for 30 min. After clearing by centrifugation at 10,000*g* for 10 min at 4°C, the supernatants were used as cell lysates for pull-down experiments using streptavidin-agarose beads (EZview, catalog no. 5529, Sigma) as described in the manufacturer's manual. Proteins were then separated by SDS-PAGE, blotted onto a nitrocellulose membrane, and detected with CtsZ or CtsB antibodies (R&D Systems).

Cell surface staining of CtsZ

Wild-type and *CtsZ*$^{-/-}$ BTCs were grown to confluency on glass coverslips (BD Biosciences). After exposure to either serum-free medium or wild-type or *CtsZ*$^{-/-}$ CM from macrophages, cells were fixed in 95% ice-cold ethanol for 7 min without subsequent cell permeabilization. Cells were then extensively rinsed in PBS and blocked with PNB for 2 h prior to overnight incubation with the CtsZ and β-catenin antibodies followed by secondary antibody labeling using a donkey anti-goat Alexa 564 antibody. Samples were mounted as previously detailed, and the numbers of CtsZ^{+} cells relative to the total cell number were determined using TissueQuest software. Representative images of the different treatment conditions were acquired using an upright Leica SP-5 confocal microscope with a 63× oil objective.

Statistical analysis

Data are expressed throughout as mean and SEM. Results were analyzed by an unpaired two-tailed Student's *t*-test unless otherwise noted and were considered statistically significant if $P < 0.05$. For the invasion analysis, a cumulative logit model (McCullagh 1980) with generalized estimating equations to correct for correlations within individual mice was used to compare the distribution of tumor types in the control group with the distribution of tumors in the experimental groups.

Acknowledgments

We thank X. Chen, K. Simpson, and A. Buck for excellent technical support, and members of the Joyce laboratory for comments and discussion. We thank Filippo Giancotti, Daniela Quail, and Oakley Olson for insightful feedback on the manuscript. We are grateful for help from Ke Xu and the MSKCC Molecular Cytology core facility, Ouathek Ouerfelli and the MSKCC Organic Synthesis core facility, and Elyn Reidel (MSKCC Biostatistics Department) for assistance with statistical analyses. We thank Dr. Nancy Du and Dr. Harold Varmus for generously providing the RIP-*Tva* animals and for experimental advice. This research was supported by the following: the National Cancer Institute (NIH R01-CA125162) and a American Cancer Society Research Scholar grant (RSG-12-076-01-LIB; J.A.J.), fellowships from the MSKCC Brain Tumor Center and American Brain Tumor Association (L.A.), a Geoffrey Beene fellowship (V.G.), Deutsche Forschungsgemeinschaft (L.S.), the graduate training programs of Weill-Cornell Medical School (V.G. and H.-W.W.), the Gerstner Sloan-Kettering Graduate School (K.E.H.), and the SFB 850 project B7 (C.P. and T.R.). L.A., V.G., and J.A.J. designed experiments and analyzed data. L.A., V.G., J.C.K., K.E.H., M.L.Q., L.S., and H.-W.W. performed experiments. L.H.T., D.S.K., T.R., and C.P. provided patient samples or reagents. J.A.J. conceived and supervised the study. L.A. and J.A.J. wrote the manuscript. All authors edited or commented on the manuscript.

References

Ashkar S, Weber GF, Panoutsakopoulou V, Sanchirico ME, Jansson M, Zawaideh S, Rittling SR, Denhardt DT, Glimcher MJ, Cantor H. 2000. Eta-1 (osteopontin): an early component of type-1 (cell-mediated) immunity. *Science* **287:** 860–864.

Bernhardt A, Kuester D, Roessner A, Reinheckel T, Krueger S. 2010. Cathepsin X-deficient gastric epithelial cells in co-culture with macrophages: characterization of cytokine response and migration capability after *Helicobacter pylori* infection. *J Biol Chem* **285:** 33691–33700.

Biswas SK, Allavena P, Mantovani A. 2013. Tumor-associated macrophages: functional diversity, clinical significance, and open questions. *Semin Immunopathol* **35:** 585–600.

Byron A, Morgan MR, Humphries MJ. 2010. Adhesion signalling complexes. *Curr Bio* **20:** R1063–R1067.

Desgrosellier JS, Cheresh DA. 2010. Integrins in cancer: biological implications and therapeutic opportunities. *Nat Rev Cancer* **10:** 9–22.

Deussing J, von Olshausen I, Peters C. 2000. Murine and human cathepsin Z: cDNA-cloning, characterization of the genes and chromosomal localization. *Biochim Biophys Acta* **1491:** 93–106.

Du YC, Lewis BC, Hanahan D, Varmus H. 2007. Assessing tumor progression factors by somatic gene transfer into a mouse model: Bcl-xL promotes islet tumor cell invasion. *PLoS Biol* **5:** e276.

Efrat S, Linde S, Kofod H, Spector D, Delannoy M, Grant S, Hanahan D, Baekkeskov S. 1988. β-Cell lines derived from transgenic mice expressing a hybrid insulin gene-oncogene. *Proc Natl Acad Sci* **85:** 9037–9041.

Fisher GH, Orsulic S, Holland E, Hively WP, Li Y, Lewis BC, Williams BO, Varmus HE. 1999. Development of a flexible and specific gene delivery system for production of murine tumor models. *Oncogene* **18:** 5253–5260.

Fonovic M, Turk B. 2014. Cysteine cathepsins and extracellular matrix degradation. *Biochim Biophys Acta* **1840:** 2560–2570.

Friedl P, Wolf K. 2010. Plasticity of cell migration: a multiscale tuning model. *J Biol Chem* **188:** 11–19.

Friedl P, Locker J, Sahai E, Segall JE. 2012. Classifying collective cancer cell invasion. *Nat Cell Biol* **14:** 777–783.

Gabarra-Niecko V, Schaller MD, Dunty JM. 2003. FAK regulates biological processes important for the pathogenesis of cancer. *Cancer Metastasis Rev* **22:** 359–374.

Gocheva V, Joyce JA. 2007. Cysteine cathepsins and the cutting edge of cancer invasion. *Cell Cycle* **6:** 60–64.

Gocheva V, Zeng W, Ke D, Klimstra D, Reinheckel T, Peters C, Hanahan D, Joyce JA. 2006. Distinct roles for cysteine cathepsin genes in multistage tumorigenesis. *Genes Dev* **20:** 543–556.

Gocheva V, Chen X, Peters C, Reinheckel T, Joyce JA. 2010a. Deletion of cathepsin H perturbs angiogenic switching, vascularization and growth of tumors in a mouse model of pancreatic islet cell cancer. *Biol Chem* **391:** 937–945.

Gocheva V, Wang HW, Gadea BB, Shree T, Hunter KE, Garfall AL, Berman T, Joyce JA. 2010b. IL-4 induces cathepsin protease activity in tumor-associated macrophages to promote cancer growth and invasion. *Genes Dev* **24:** 241–255.

Greenbaum D, Medzihradszky KF, Burlingame A, Bogyo M. 2000. Epoxide electrophiles as activity-dependent cysteine protease profiling and discovery tools. *Chem Biol* **7:** 569–581.

Hanahan D. 1985. Heritable formation of pancreatic β-cell tumours in transgenic mice expressing recombinant insulin/simian virus 40 oncogenes. *Nature* **315:** 115–122.

Hanahan D, Coussens LM. 2012. Accessories to the crime: functions of cells recruited to the tumor microenvironment. *Cancer Cell* **21:** 309–322.

Hidaka S, Yasutake T, Takeshita H, Kondo M, Tsuji T, Nanashima A, Sawai T, Yamaguchi H, Nakagoe T, Ayabe H, et al. 2000. Differences in 20q13.2 copy number between colorectal cancers with and without liver metastasis. *Clin Cancer Res* **6:** 2712–2717.

Himly M, Foster DN, Bottoli I, Iacovoni JS, Vogt PK. 1998. The DF-1 chicken fibroblast cell line: transformation induced by diverse oncogenes and cell death resulting from infection by avian leukosis viruses. *Virology* **248:** 295–304.

Hu W, Feng Z, Modica I, Klimstra DS, Song L, Allen PJ, Brennan MF, Levine AJ, Tang LH. 2010. Gene amplifications in well-differentiated pancreatic neuroendocrine tumors inactivate the p53 pathway. *Genes Cancer* **1:** 360–368.

Humphries JD, Byron A, Humphries MJ. 2006. Integrin ligands at a glance. *J Cell Sci* **119:** 3901–3903.

Huttenlocher A, Horwitz AR. 2011. Integrins in cell migration. *Cold Spring Harb Perspect Biol* **3:** a005074.

Hynes RO, Naba A. 2012. Overview of the matrisome—an inventory of extracellular matrix constituents and functions. *Cold Spring Harb Perspect Biol* **4:** a004903.

Jevnikar Z, Obermajer N, Bogyo M, Kos J. 2008. The role of cathepsin X in the migration and invasiveness of T lymphocytes. *J Cell Sci* **121:** 2652–2661.

Jevnikar Z, Obermajer N, Doljak B, Turk S, Gobec S, Svajger U, Hailfinger S, Thome M, Kos J. 2011. Cathepsin X cleavage of the β2 integrin regulates talin-binding and LFA-1 affinity in T cells. *J Leukoc Biol* **90:** 99–109.

Joyce JA, Pollard JW. 2009. Microenvironmental regulation of metastasis. *Nat Rev Cancer* **9:** 239–252.

Joyce JA, Baruch A, Chehade K, Meyer-Morse N, Giraudo E, Tsai FY, Greenbaum DC, Hager JH, Bogyo M, Hanahan D. 2004. Cathepsin cysteine proteases are effectors of invasive growth and angiogenesis during multistage tumorigenesis. *Cancer Cell* **5:** 443–453.

Kang Y, He W, Tulley S, Gupta GP, Serganova I, Chen CR, Manova-Todorova K, Blasberg R, Gerald WL, Massague J. 2005. Breast cancer bone metastasis mediated by the Smad tumor suppressor pathway. *Proc Natl Acad Sci* **102:** 13909–13914.

Ke N, Wang X, Xu X, Abassi YA. 2011. The xCELLigence system for real-time and label-free monitoring of cell viability. *Methods Mol Biol* **740:** 33–43.

Kos J, Jevnikar Z, Obermajer N. 2009. The role of cathepsin X in cell signaling. *Cell Adhes Migr* **3:** 164–166.

Krueger S, Kalinski T, Hundertmark T, Wex T, Kuster D, Peitz U, Ebert M, Nagler DK, Kellner U, Malfertheiner P, et al. 2005. Up-regulation of cathepsin X in *Helicobacter pylori* gastritis and gastric cancer. *J Pathol* **207:** 32–42.

Lechner AM, Assfalg-Machleidt I, Zahler S, Stoeckelhuber M, Machleidt W, Jochum M, Nagler DK. 2006. RGD-dependent binding of procathepsin X to integrin αvβ3 mediates cell-adhesive properties. *J Biol Chem* **281:** 39588–39597.

Limame R, Wouters A, Pauwels B, Fransen E, Peeters M, Lardon F, De Wever O, Pauwels P. 2012. Comparative analysis of dynamic cell viability, migration and invasion assessments by novel real-time technology and classic endpoint assays. *PLoS ONE* **7:** e46536.

Lines KE, Chelala C, Dmitrovic B, Wijesuriya N, Kocher HM, Marshall JF, Crnogorac-Jurcevic T. 2012. S100P-binding protein, S100PBP, mediates adhesion through regulation of cathepsin Z in pancreatic cancer cells. *Am J Pathol* **180:** 1485–1494.

Lopez T, Hanahan D. 2002. Elevated levels of IGF-1 receptor convey invasive and metastatic capability in a mouse model of pancreatic islet tumorigenesis. *Cancer Cell* **1:** 339–353.

Lu P, Weaver VM, Werb Z. 2012. The extracellular matrix: a dynamic niche in cancer progression. *J Biol Chem* **196:** 395–406.

McCullagh P. 1980. Regression models for ordinal data. *J R Stat Soc [Ser A]* **42:** 109–142.

Mitra SK, Schlaepfer DD. 2006. Integrin-regulated FAK–Src signaling in normal and cancer cells. *Curr Opin Cell Biol* **18:** 516–523.

Mohamed MM, Sloane BF. 2006. Cysteine cathepsins: multifunctional enzymes in cancer. *Nat Rev Cancer* **6:** 764–775.

Moreno-Layseca P, Streuli CH. 2014. Signalling pathways linking integrins with cell cycle progression. *Matrix Biol* **34C:** 144–153.

Nagaraj NS, Smith JJ, Revetta F, Washington MK, Merchant NB. 2010. Targeted inhibition of SRC kinase signaling attenuates pancreatic tumorigenesis. *Mol Cancer Ther* **9:** 2322–2332.

Nagler DK, Menard R. 1998. Human cathepsin X: a novel cysteine protease of the papain family with a very short proregion and unique insertions. *FEBS Lett* **434:** 135–139.

Nagler DK, Zhang R, Tam W, Sulea T, Purisima EO, Menard R. 1999. Human cathepsin X: a cysteine protease with unique carboxypeptidase activity. *Biochemistry* **38:** 12648–12654.

Nagler DK, Kruger S, Kellner A, Ziomek E, Menard R, Buhtz P, Krams M, Roessner A, Kellner U. 2004. Up-regulation of cathepsin X in prostate cancer and prostatic intraepithelial neoplasia. *Prostate* **60:** 109–119.

Noy R, Pollard JW. 2014. Tumor-associated macrophages: from mechanisms to therapy. *Immunity* **41:** 49–61.

Obermajer N, Repnik U, Jevnikar Z, Turk B, Kreft M, Kos J. 2008a. Cysteine protease cathepsin X modulates immune response via activation of β2 integrins. *Immunology* **124:** 76–88.

Obermajer N, Svajger U, Bogyo M, Jeras M, Kos J. 2008b. Maturation of dendritic cells depends on proteolytic cleavage by cathepsin X. *J Leukoc Biol* **84:** 1306–1315.

Okabe M, Ikawa M, Kominami K, Nakanishi T, Nishimune Y. 1997. 'Green mice' as a source of ubiquitous green cells. *FEBS Lett* **407:** 313–319.

Palermo C, Joyce JA. 2008. Cysteine cathepsin proteases as pharmacological targets in cancer. *Trends Pharmacol Sci* **29:** 22–28.

Pyonteck SM, Akkari L, Schuhmacher AJ, Bowman RL, Sevenich L, Quail DF, Olson OC, Teijeiro V, Setty M, Leslie C, et al. 2013. CSF-1R inhibition alters macrophage polarization and blocks gliomagenesis. *Nat Med* **19:** 1264–1272.

Quail DF, Joyce JA. 2013. Microenvironmental regulation of tumor progression and metastasis. *Nat Med* **19:** 1423–1437.

Sangaletti S, Di Carlo E, Gariboldi S, Miotti S, Cappetti B, Parenza M, Rumio C, Brekken RA, Chiodoni C, Colombo MP. 2008. Macrophage-derived SPARC bridges tumor cell-extracellular matrix interactions toward metastasis. *Cancer Res* **68:** 9050–9059.

Santamaria I, Velasco G, Pendas AM, Fueyo A, Lopez-Otin C. 1998. Cathepsin Z, a novel human cysteine proteinase with a short propeptide domain and a unique chromosomal location. *J Biol Chem* **273:** 16816–16823.

Sevenich L, Joyce JA. 2014. Pericellular proteolysis in cancer. *Genes Dev* (in press).

Sevenich L, Schurigt U, Sachse K, Gajda M, Werner F, Muller S, Vasiljeva O, Schwinde A, Klemm N, Deussing J, et al. 2010. Synergistic antitumor effects of combined cathepsin B and cathepsin Z deficiencies on breast cancer progression and metastasis in mice. *Proc Natl Acad Sci* **107:** 2497–2502.

Sevenich L, Bowman RL, Mason SD, Quail DF, Rapaport F, Elie BT, Brogi E, Brastianos PK, Hahn WC, Holsinger LJ, et al. 2014. Analysis of tumour- and stroma-supplied proteolytic networks reveals a brain-metastasis-promoting role for cathepsin S. *Nat Cell Biol* **16:** 876–888.

Sivaraman J, Nagler DK, Zhang R, Menard R, Cygler M. 2000. Crystal structure of human procathepsin X: a cysteine protease with the proregion covalently linked to the active site cysteine. *J Mol Biol* **295:** 939–951.

Slack-Davis JK, Martin KH, Tilghman RW, Iwanicki M, Ung EJ, Autry C, Luzzio MJ, Cooper B, Kath JC, Roberts WG, et al. 2007. Cellular characterization of a novel focal adhesion kinase inhibitor. *J Biol Chem* **282:** 14845–14852.

Song S, Ewald AJ, Stallcup W, Werb Z, Bergers G. 2005. PDGFRβ$^+$ perivascular progenitor cells in tumours regulate pericyte differentiation and vascular survival. *Nat Cell Biol* **7:** 870–879.

Tang LH, Contractor T, Clausen R, Klimstra DS, Du YC, Allen PJ, Brennan MF, Levine AJ, Harris CR. 2012. Attenuation of the retinoblastoma pathway in pancreatic neuroendocrine tumors due to increased cdk4/cdk6. *Clin Cancer Res* **18:** 4612–4620.

Turk V, Stoka V, Vasiljeva O, Renko M, Sun T, Turk B, Turk D. 2012. Cysteine cathepsins: from structure, function and regulation to new frontiers. *Biochim Biophys Acta* **1824:** 68–88.

Tuveson D, Hanahan D. 2011. Translational medicine: cancer lessons from mice to humans. *Nature* **471:** 316–317.

Vasiljeva O, Papazoglou A, Kruger A, Brodoefel H, Korovin M, Deussing J, Augustin N, Nielsen BS, Almholt K, Bogyo M, et al. 2006. Tumor cell-derived and macrophage-derived cathepsin B promotes progression and lung metastasis of mammary cancer. *Cancer Res* **66:** 5242–5250.

Vizin T, Christensen IJ, Nielsen HJ, Kos J. 2012. Cathepsin X in serum from patients with colorectal cancer: relation to prognosis. *Radiol Oncol* **46:** 207–212.

Wang J, Chen L, Li Y, Guan XY. 2011. Overexpression of cathepsin Z contributes to tumor metastasis by inducing epithelial-mesenchymal transition in hepatocellular carcinoma. *PLoS ONE* **6:** e24967.

Xiong J, Balcioglu HE, Danen EH. 2013. Integrin signaling in control of tumor growth and progression. *Int J Biochem Cell Biol* **45:** 1012–1015.

Distinct functions of macrophage-derived and cancer cell-derived cathepsin Z combine to promote tumor malignancy via interactions with the extracellular matrix

Leila Akkari, Vasilena Gocheva, Jemila C. Kester, et al.

Genes Dev. 2014, **28:**
Access the most recent version at doi:10.1101/gad.249599.114